DEVELOPMENT OF AN EFFECTIVE COMPUTATIONAL METHODOLOGY FOR MULTI-STAGE COMPRESSOR MAP GENERATION

by

TAEK JIN CHOI

B.S. Mechanical Engineering, Carnegie Mellon University, 1997
M.S. Mechanical Engineering, Carnegie Mellon University, 1999

Submitted to the Department of Aeronautics and Astronautics
in partial fulfillment of the requirements for the degree of

MASTER OF SCIENCE

at the

MASSACHUSETTS INSTITUTE OF TECHNOLOGY

September 2001

Author _____
Department of Aeronautics and Astronautics
July 27, 2001

Certified by _____
Dr. Choon Sooi Tan
Senior Research Engineer
Thesis Supervisor

Accepted by _____
Professor Wallace Earl Vander Velde
Professor of Aeronautics and Astronautics
Chair, Committee on Graduate Students

DEVELOPMENT OF AN EFFECTIVE COMPUTATIONAL METHODOLOGY FOR MULTI-STAGE COMPRESSOR MAP GENERATION

by

TAEK JIN CHOI

Submitted to the Department of Aeronautics and Astronautics on July 27, 2001
in partial fulfillment of the requirements for the degree of
Master of Science

ABSTRACT

A framework for effective computational methodology was developed for multi-stage compressor map generation. The methodology consists of using a few isolated-blade row Navier-Stokes solutions for each blade row to construct a body force database. The purpose of the body force database is to replace each blade row in a multi-stage compressor by a body force distribution to produce same pressure rise and flow turning. To do this, each body force database is generated in such a way that it can respond to the changes in local flow conditions. Once the database is generated, no further Navier-Stokes computations are necessary. The process is repeated for every blade row in the multi-stage compressor. The body forces are then embedded as source terms in an Euler solver. The method is developed to have the capability to compute the performance in a flow that has radial as well as circumferential non-uniformity with a length scale larger than a blade pitch; thus it can potentially be used to characterize the stability of a compressor under design. It is these two latter features as well as the procedure to obtain the body force representation that distinguish the present methodology from the streamline curvature method.

The overall computational procedures have been developed. A dimensional analysis was carried out to determine the local flow conditions for parameterizing the magnitudes of the local body force representation of blade rows. An Euler solver was modified to embed the body forces as source terms. Four test cases were performed to validate and assess the current methodology.

The results from the dimensional analysis show that the body forces can be parameterized in terms of the two relative flow angles, the relative Mach number, and the Reynolds number. For the flow in a high-speed transonic blade row, they can be parameterized in terms of the local relative Mach number alone. It is deduced that the performance and the flow distribution of a single blade row subjected to radial inlet distortions can be predicted using the body force database created from the Navier-Stokes solutions with uniform inlet conditions. Likewise, the performance at an operating point, other than those from which the database for the body forces were extracted, can be computed as well.

Thesis Supervisor: Dr. Choon S. Tan
Title: Senior Research Engineer

ACKNOWLEDGEMENTS

I would like to express my gratitude to Dr. Choon S. Tan for giving me an opportunity to work on this exciting research project. I also wish to thank Dr. Yifang Gong for giving me a version of his Euler code, guidance, and insightful comments, and Mr. Jim Bleeg of Pratt & Whitney Aircraft Engine for proving me with invaluable RANS solutions. I am indebted to Professor Frank E. Marble of California Institute of Technology and Professor Nick A. Cumpty of Whittle Laboratory at Cambridge University for their inputs on this work.

Without a doubt, the graduate students of MIT Gas Turbine Laboratory have made my two years of MIT experience a pleasant one. I especially thank Duc Vo and Bobby Sirakov for interesting conversations about life, culture, and politics. Coffee breaks with Dongwon and Hyung-soo helped me stay awake for debugging the computer programs and running numerical computations. I also would to thank Simon Evans, Zack Warfield, and Laurent Jamonet for being wonderful officemates.

I would also like to take this opportunity to thank Professor Tom I-P. Shih of the Engine Laboratory at Michigan State University for introducing me to the fascinating field of computational fluid dynamics when I was an undergraduate student at Carnegie Mellon University. I have benefited enormously from his constant motivations, guidance, and insights for excellence. Without him, I would not have made it this far.

Finally, I would like to dedicate this thesis to my mother, Sun Hae Choi, for her enormous sacrifice and forbearance while I pursued my undergraduate and two graduate degrees for the last eight years.

This research was supported by a MIT Presidential Graduate Fellowship, Pratt & Whitney Aircraft Engine under Contract Agreement Number 98-023 with Drs. Mark Barnett and Bob Ni, and Mr. Mark Aubuchon as technical monitors, and NASA Glenn Research Center under Grant Number NAS3-2101 with Dr. Ken Suder as technical monitor. Their support is gratefully acknowledged.

CONTENTS

LIST OF FIGURES

LIST OF TABLES

CHAPTER 1

INTRODUCTION

1.1 Background

Considerable advances in compressor design methodologies have been made since the first gas turbine aircraft engines were developed in late 1930s and early 1940s. Designs have been developed based on one-dimensional mean-line analyses coupled with cascade data, and they often involved numerous iterations between design and testing until satisfactory configurations were found. Radial Equilibrium and Streamline Curvature methods [3], [18], [22], brought the analytical design method from one to two dimensions (axi-symmetric), and led to improved first bench test performance. By 1970s, the two-dimensional methods were matured considerably and used extensively in industry for complete engine analyses and designs. Such methods have enabled the designers to reduce the number of design iterations for engine product development.

The aerodynamic performance of a compressor from design or testing is given as a plot of pressure rise as a function of corrected mass flow rate for each compressor speed. Such a figure is known as a *compressor performance map*. Further analyses such as compressor stability analysis using the compressor performance characteristics are possible.

A point of instability is reached at which the pressure rise is a maximum and further reduction in mass flow leads to an abrupt and dramatic change in the flow pattern in the

compressor. Once a series of the instability points are identified for a range of operating speed, they are connected by what is called a *surge line*. The surge line is defined by the limit in pressure ratio, for each compressor speed, beyond which the flow in the compressor breaks down in some way so as to make the system no longer operable [11]. Predicting the condition at which instability will occur in a compressor is an essential part of the design process.

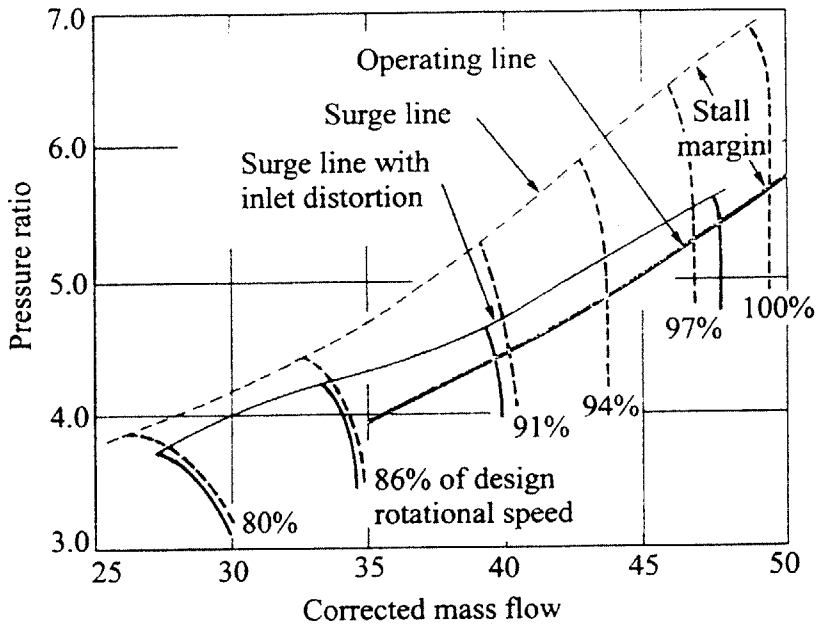

Figure 1.1: Compressor performance map and the effects of inlet distortions [19]

When the compressor map for a design is first generated, either numerically or experimentally, it represents the compressor performance under normal operating conditions. However, there are many uncertainties related to instability: uncertainties of prediction for a given design and uncertainties associated with the conditions of operation. Uncertainties of operation include inlet distortions (Figure 1.1), which may be transient; transient throttle changes, such as occur when an engine is accelerated; transient geometry changes such as tip and axial clearance changes following speed

changes; and compressor mechanical damage including blade erosion and the effects of large foreign body ingestion [3]. Predictions of the compressor performance under all those uncertainties are difficult, if not impossible. However, such capability will enable compressor designers to quantify stability characteristics of compressor designs related to the uncertainties and make significant performance improvements.

During the past two decades, computational fluid dynamics (CFD) has been playing an increasing role in the development and advancement of compressor design and analysis. Modern design methods can, in principle and to some extent in practice, utilize CFD results rather than experiments [13]. This is due to the increasing availability in computer resources (speed, memory, and data storage) and the considerable advances made in CFD algorithm. Figure 1.2 depicts a typical empirically-based design system tied to a two-dimensional CFD analysis tool. A key goal in industry today is to develop a three-dimensional computer-based compressor design and achieve the expected performance at the first bench test.

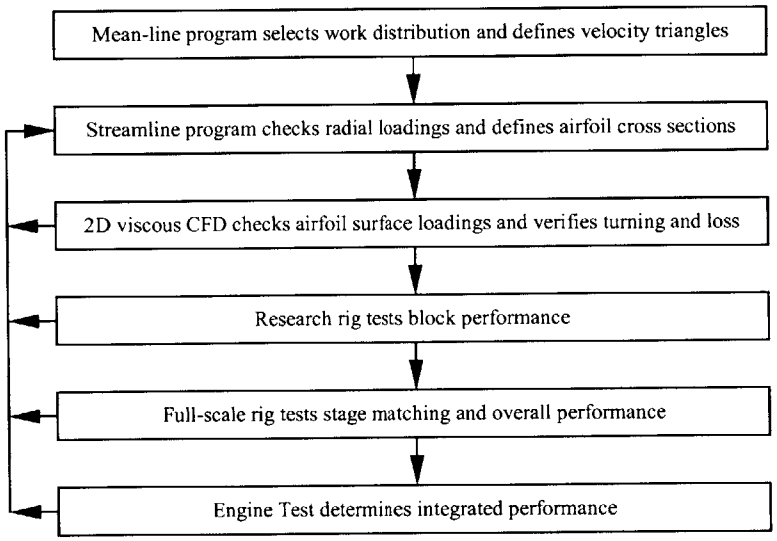

Figure 1.2: Empirically-based compressor design system [13]

The increasing computing power has enabled computations of three-dimensional flow in turbomachines. Such computations, applied to single blade rows or single stages, have led to considerable reduction in compressor design time cycles, and have helped develop innovative ideas for blade designs leading to substantial performance improvements [13]. However, three-dimensional Navier-Stokes computations in a multi-stage compressor are not yet achievable in amounts of time acceptable for design purposes without massive parallel computing resources. A compressor design system based on three-dimensional Navier-Stokes calculations is shown in Figure 1.3.

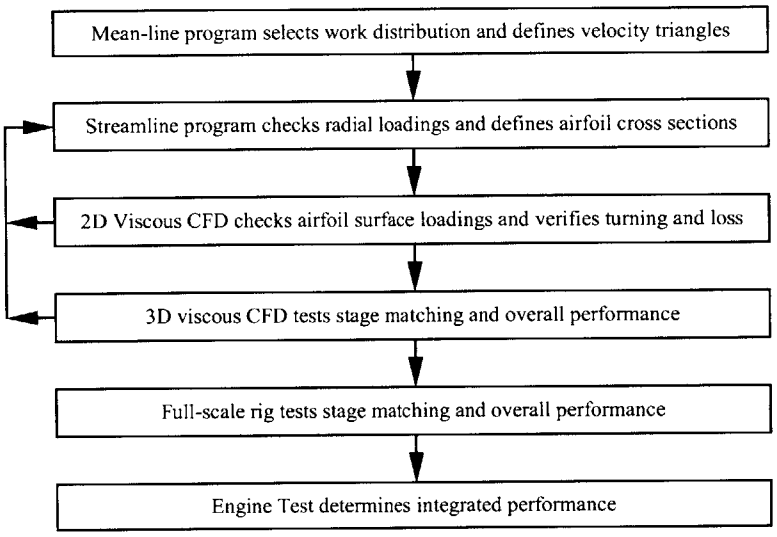

Figure 1.3: Three-dimensional Navier-Stokes calculation-based compressor design system [13]

1.2 Motivation of the Research

As direct multi-stage computations cannot be used for multi-stage compressor designs, approximations that are adequate for design and analysis purpose must be made between two neighboring blade rows. One of the most commonly used approximations is the

mixing plane approach [5]. For example, in the process of using this approach, the rotor is first designed using the mixed-out upstream conditions of the downstream stator as the outflow boundary conditions. The mixed-out rotor outflow conditions are then used as the inflow boundary conditions for the downstream stator design (see Figure 1.4). Since each blade row is designed individually, this leads to an essentially steady design method that does not reflect the impact of any unsteady phenomenon on the compressor performance.

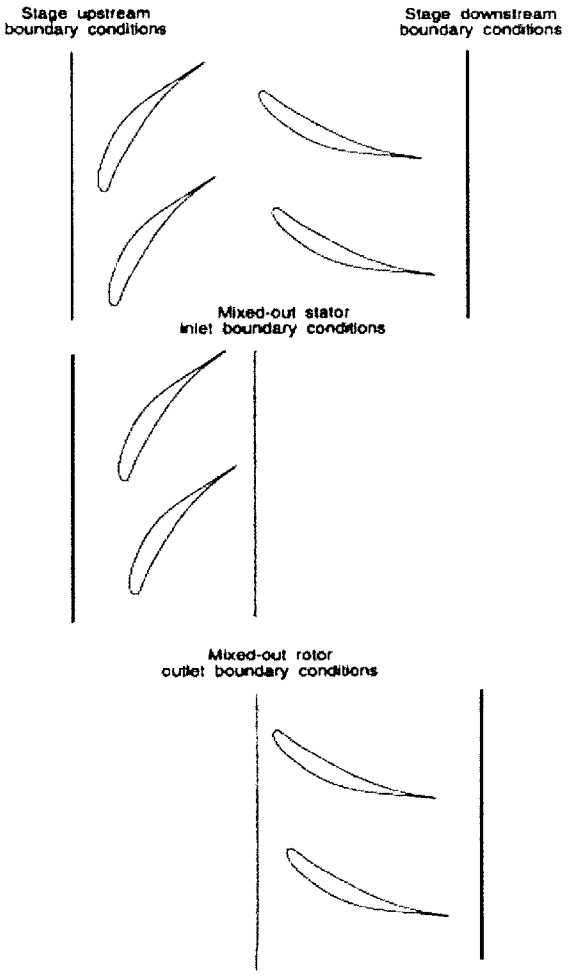

Figure 1.4: Mixing plane approach [26]

However, it has been known that unsteady interactions between two adjacent blade rows can play an important role in determining the maximum pressure rise and efficiency of a compressor. It has been shown that blade row spacing between two blade rows has a significant impact on the compressor performance [9], [16], [23].

For this reason, there [21] has been an attempt to implement an approximate technique for incorporating periodic unsteadiness by modifying the average passage approach of Adamczyk [1], [17], which employs the concept of *body forces* and *deterministic stresses* (see Figure 1.5). In this method, the body forces introduce a potential interference effect by establishing a "target" radial static pressure profile at the interface plane between closely coupled rows, and the deterministic stresses account for the "average" wake blockage and mixing effects both axially and radially. This new approach has been shown to be effective in incorporating the unsteady interaction phenomena into a multi-stage compressor design. However, a full three-dimensional Navier-Stokes computation for an entire multi-stage compressor is still required to use it, with considerable computing resources.

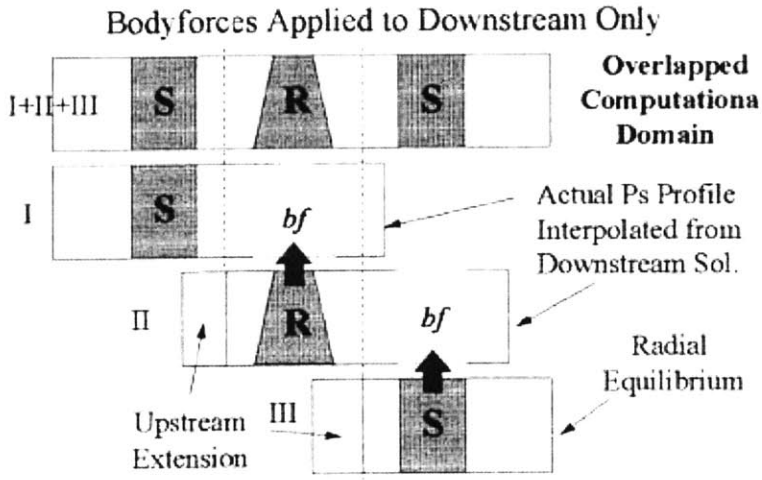

Figure 1.5: Average passage approach with body forces and deterministic stresses [21]

Several mechanisms of blade row interaction, and their impact on compressor performance, have been studies previously. The reader should refer to the work by Valkov [25] for a comprehensive review about the mechanisms. In general, the blade row interaction can be classified in two types: potential and vortical. Potential interaction is the impact of the blade row pressure field on the upstream and downstream blade rows. Vortical interaction represents the effect of vortical structures, e.g. wake, tip vortex, stream-wise and corner vortices, on downstream blade rows. Both forms have been shown, analytically and experimentally, to have impact on the compressor performance.

Even though these mechanisms have been studied in the past, this has only been done on the level of a single compressor stage and thus the overall impact of the mechanisms on the level of the entire multistage compressor has not been yet quantified.

Thus, there is a need for an adequate and effective methodology for the generation of multi-stage compressor performance map. This new methodology should (1) incorporate the correct flow interaction phenomena between two neighboring blade rows in a multi-stage compressor, (2) generate multi-stage compressor map for performance evaluation on an effective and adequate basis, and (3) achieve the aforementioned goals with computationally manageable resources.

Hence, the overall goal of the research is to develop and demonstrate an adequate and effective methodology for multi-stage compressor computations that yield compressor maps for design purposes.

1.3 A Brief Review of Previous Work on Use of Body Forces in Turbomachinery

The concept of using body force distribution to represent a blade row is not new. It has been used by Marble [15], Horlock and Marsh [10], Denton [4], and Adamczyk [1] among others. Escuret and Garnier [6], Longley [14], and Gong [8] have recently used body force distributions to simulate instability inception in a low-speed multi-stage compressor by long- and short-wavelength disturbances.

Marble has developed an axisymmetric body force model for through-flow computations in blade rows. This body force can be viewed as the distribution of the force applied by the blade on the flow, which can be decomposed into a normal pressure force and a tangential shear force. Marble's model can be implemented if the blade geometry and various flow variables at the blade surface are known.

Horlock and Marsh showed, by averaging the two-dimensional differential form of the continuity and momentum equations across a blade passage, that two-dimensional blade rows in steady inviscid flow can be replaced by distributed body forces. The computation of their body forces requires the knowledge of the static pressure on the blade surface.

Denton used distributed stream-wise body forces to simulate viscous effects in a flow otherwise computed using an inviscid solver. He showed that the pitch-wise profile of body forces could be arbitrarily chosen, provided they create the correct shear force at the blade surface, which is the input in the construction of his model.

Adamczyk showed by applying three averaging operators on the three-dimensional unsteady Navier-Stokes equations that unsteadiness resulting from a multi-blade row environment can be captured on an averaged basis by a steady computation using distributed body forces, heat sources and deterministic stresses. The model elements are

obtained by the application of a closure model, in the same way as a turbulence model is used to obtain Reynolds stresses in a turbulent flow computation.

Escuret and Garnier demonstrated the capability of using a body force distribution for simulating the development of instabilities in multi-stage axial compressors. They used a three-dimensional unsteady Euler code coupled with the body force distribution based on multiple through-flow solutions within blade rows. The model was developed for predicting the growth of only long-wavelength instabilities.

Longley developed a computational model for the moderate to long-wavelength instabilities of high-speed multi-stage compressors. In his work, the flow outside the blade rows was computed using a two-dimensional Euler solver while the individual blade rows were modeled using multiple one-dimensional flow fields with body force distributions.

Gong had developed a model for simulating axial compressor stall inception associated with both long- and short-wavelength disturbances. Individual blade rows were represented by a body force distribution formulated in terms of the blade's pressure rise and flow turning characteristics. The computational model uses a body force distribution that responds to local flow conditions. To achieve this, knowledge about the compressor performance and geometry must be known prior to modeling.

1.4 A Comment on Present Methodology vs. Streamline Curvature

As alluded to in the above, current/modern thinking on stability modeling involves viewing a compressor blade row as a body force distribution. In the past, the body force representation was based on correlation and meanline analysis as was implemented in streamline curvature and throughflow methods in implicit terms. However, the present

proposed methodology, to be described later, explicitly obtains the body force representation of each blade row in a multi-stage compressor from the "best" available three-dimensional Navier-Stokes solver on a physically consistent basis.

Whereas a streamline curvature method or throughflow analysis is only capable of computing turbomachinery performance in a flow with radial flow variations, the technical framework under which the present proposed methodology is implemented in such that it can compute the performance in a flow that has radial as well as circumferential variations (with length-scales larger than the blade pitch). As such, it can potentially be used to characterize the stability of a compressor under design. It is these two latter aspects, namely how body force representation of a blade row is constructed and the ability to deal with a flow with circumferential non-uniformities, that distinguish the present method from the others.

1.5 Research Objectives

The methodology to be considered and developed here consists of replacing each blade row by an equivalent body force distribution to produce correct pressure rise and flow turning. This methodology must be designed to be computationally feasible while retaining the effect on performance of the important flow features in the entire multi-stage compressor.

The research objectives are as follows:

1. To develop an adequate computational procedure for generating row-by-row body force representation of high-speed transonic compressors

2. To assess the applicability of the model for multi-stage flow analysis and design feasibility by comparing against multi blade row CFD computations

3. To enable its integration into a compressor design system for generating compressor map

Modeling is first addressed for a steady state rotor blade row under uniform inlet flow conditions to understand the key concepts. The adequacy of the model is then validated with the same configuration subjected to radial inlet distortions. The model is then extended further for an IGV-rotor-stator configuration to assess the applicability for multi-stage compressor analysis and design. Having completed these steps, the methodology will be applied for performance prediction of a compressor subjected to circumferential inlet distortions and for stability characterization.

1.6 Contributions of the Thesis

The major contributions of the present thesis are as follows:

1. A computational methodology was developed to perform numerical computations for efficient compressor map generation. The methodology consists of developing computer programs to generate a pitch-wise-averaged body force distribution from isolated blade row Navier-Stokes solutions by considering an integral form of the momentum equation for each control volume.

2. A dimensional Analysis using the Π-Theorem was performed to identify the key parameters that can parameterize the local body forces. They are the two local flow angles (radial and tangential), local relative Mach number, and Reynolds number. For a high-speed transonic compressor, it was deduced that the body forces are only a function of the local relative Mach number. Multiple Navier-Stokes solutions for an isolated high-speed blade row were

used to parameterize the forces and construct a body force database based on this conclusion. The database enables the body forces to responds to the local flow condition.

3. The implementation of the model was validated with several test cases by performing numerical computations of a rotor blade row and by comparing the corresponding solutions against the original Navier-Stokes solutions. It was demonstrated that the body force database created from isolated blade row calculations is able to accurately predict the performance of a single blade row subjected to radial inlet distortions based on the computational results obtained from the test cases. Furthermore, the applicability of the computational model developed in this thesis was shown to be encouraging for a multi-stage compressor. The computational methodology is expected to predict the performance of the blade row subjected to circumferential inlet distortions and for detailed stability characterization associated with both long- and short-wave disturbances.

1.7 Organization of the Thesis

The main ideas associated with the body force formulation are first illustrated by the presentation of the physical concepts and the development of a basic computational model in Chapter 2.

In Chapter 3, new capabilities added to the existing model are assessed and validated via the following two levels: *local* and *system level*. On the local level, the applicability of the model is first assessed by an extraction of the appropriate body force representation of an isolated blade row and subsequently by a successful replication of the flow field by applying the new representation. Having accomplished the first step, a dimensional analysis is carried out to identify a set of local flow parameters that set the magnitudes of

the forces. The use of this set of the local flow parameters for correlating the response of the body forces with respect to the changes in local flow conditions is illustrated for a blade row subjected to a non-uniform inlet flow.

The model is then further extended to the system level. On this level, adequacy of the body force formulation for multi-stage compressor map generation is assessed by the reconstruction of the flow field in an entire multi-stage compressor by the use of the body force distributions extracted from isolated blade row calculations of individual blade rows in the compressor. The main goal of this level is to demonstrate if uncoupled isolated blade row calculations can be employed to construct an accurate and physically meaningful flow field in the multi-stage compressor.

In Chapter 4, four test cases considered for the validation of the concepts developed on the local and system levels are described, and the corresponding results and discussions are provided in Chapter 5.

Finally, summary and conclusions are presented on the overall performance of the computational methodology are presented in Chapter 6, and guidelines are provided for future work.

CHAPTER 2

DEVELOPMENT OF COMPUTATIONAL METHODOLOGY: PART I

2.1 Introduction

The first part of the computational methodology using the body force formulation developed in the present research is described in this chapter. Preliminary concepts and basic problem formulations are covered in this part of the development process. Direct extensions of the concepts, formulations, and further analyses are presented in Chapter 3. The first part consists of (1) presenting the main idea of a body force formulation; (2) major advantages of using the body force formulation over standard computational methodologies that are currently being used in industry for multi-stage simulations; (3) overall computational procedure involved to assess the degree of validity of the basic body force concept; (4) steps involved for extracting the body forces; (5) formulation of the new governing equations for the flows in ducts and in blade row regions; (6) presenting the numerical methods of solutions; and (7) a summary.

2.2 Body Force Formulation

As it was mentioned in the introduction, the first part of the computational methodology begins with the presentation of the body force formulation. A simple graphical

representation is shown in Figure 2.1. Figure 2.1(a) represents a conventional CFD approach, e.g. three-dimensional Navier-Stokes analysis, to compute the flow in a blade row. Figure 2.1(b) shows the axi-symmetric Euler approach with the basic body force representation to produce the identical flow turning and total-pressure rise: the effects of the blade geometries are replaced by equivalent local body forces. Figure 2.2 illustrates the body force methodology in a three-dimensional view. At each point within the blade row, the body forces can conveniently be described in terms of their three components: F_x, F_θ, F_r, i.e. the axial, tangential, and radial forces, respectively, or a component normal to the flow and a component parallel to the flow.

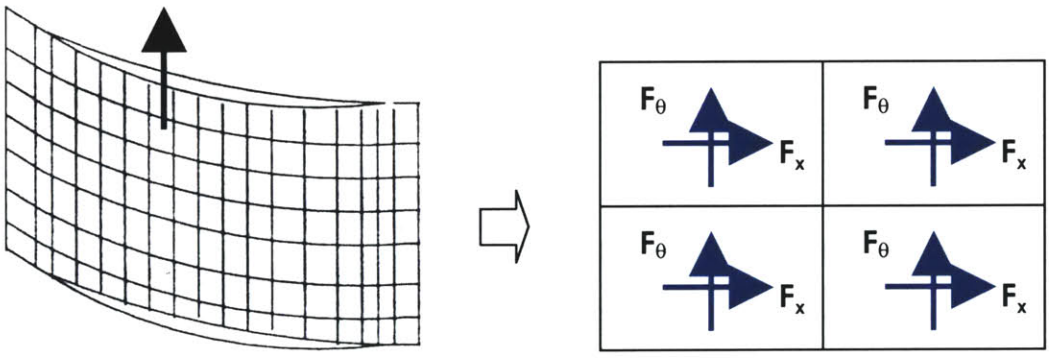

(a) (b)

Figure 2.1: Computational methodology: (a) conventional CFD approach and (b) axi-symmetric Euler with body force approach

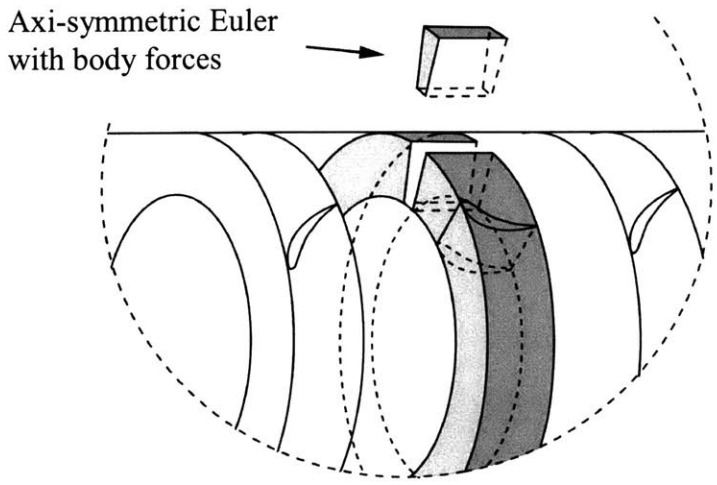

Figure 2.2: Three-dimensional illustration of the model using the body force distributions [8]

2.3 Main Advantages of Model

There are many advantages of using the axi-symmetric Euler with the body force approach over conventional CFD methodologies based on three-dimensional Navier-Stokes equations. However, two key advantages are described in this section. Replacing the blade rows in a multi-stage compressor by the equivalent body force distributions leads to significant improvements in terms of computational costs. The rest of the section is devoted to provide the explanation for the claim.

First, the new computational methodology makes use of an axi-symmetric Euler CFD code with body forces embedded as source terms in the governing equations. Here, intra-blade-row regions, and upstream and downstream ducts are assumed to be inviscid, while viscous effects are accounted for inside the blade rows. Hence, the number of required grid points is significantly reduced since detailed flow features such as boundary layers,

shear forces, and tip clearance flows do not need to be resolved. However, their effects are reflected in the body force representation.

Second, an entire multi-stage compressor computation requires only one computational domain. Typically, for the conventional three-dimensional Navier-Stokes analysis, the total number of computational domains needed is equal to the number of the blade rows in a multi-stage compressor. It is because the rotor-blade-row domains rotate at an angular speed with respect to that for the stator blade rows, as illustrated in Figure 2.3.

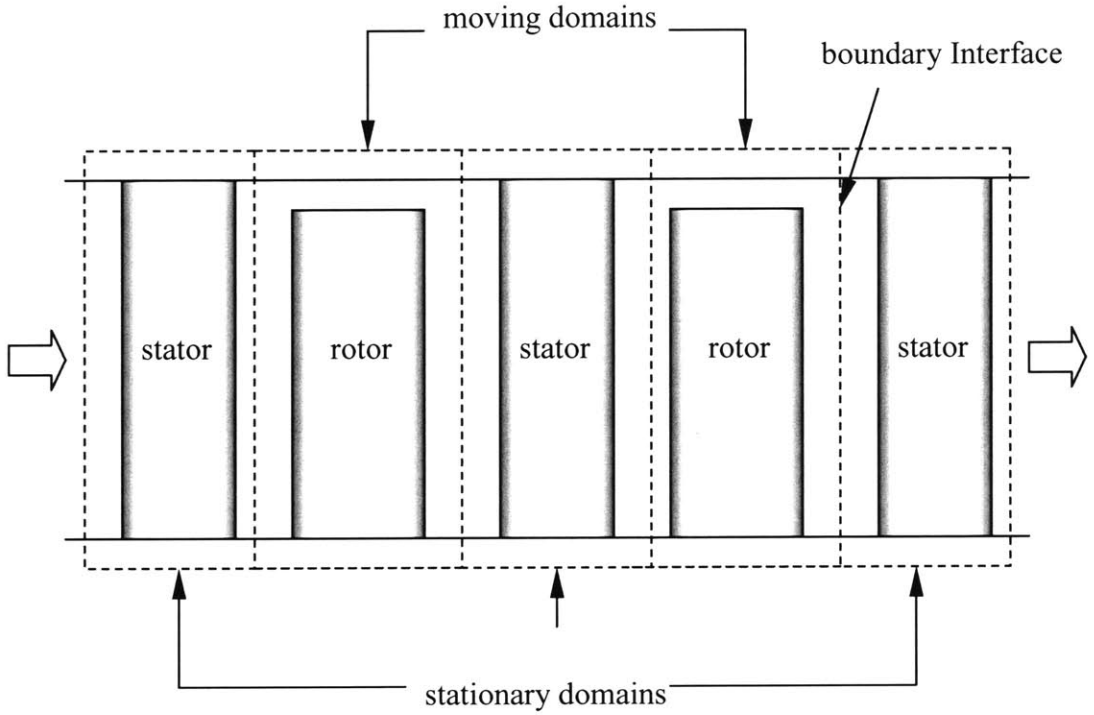

Figure 2.3: Conventional CFD multi-stage analysis: each dashed rectangle represents a computational domain.

The body force approach eliminates this requirement: the entire multi-stage compressor is modeled as one stationary annulus duct with the effects of the blade rows being substituted by the equivalent body force distributions, as shown in Figure 2.4.

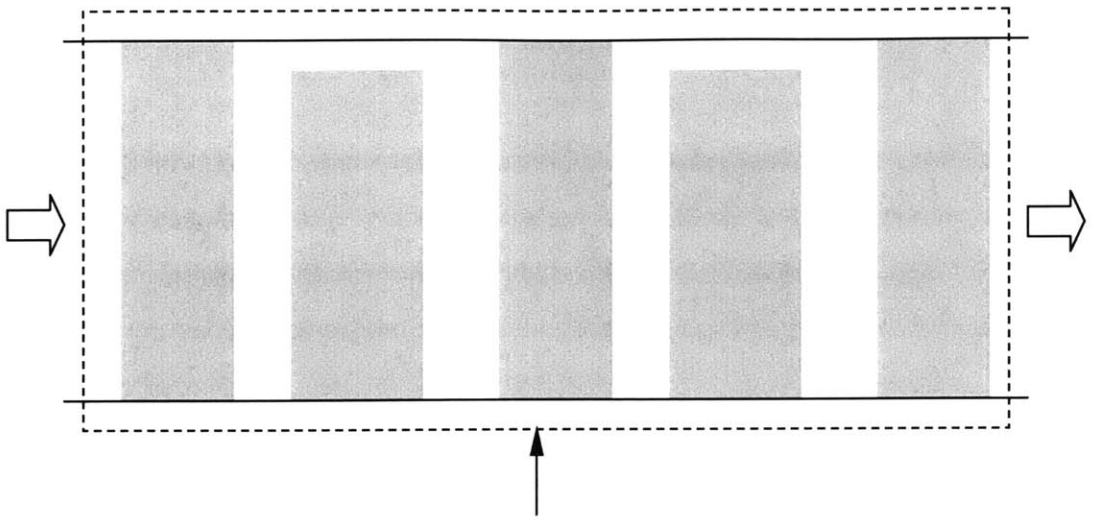

Figure 2.4: New multi-stage analysis with body force distributions: each shaded rectangle represents an equivalent body force representation of the blade. Only one computational domain is required.

2.4 Overall Computational Procedure

In this section, the overall computational procedures are presented. Two flow charts are provided to illustrate the procedures involved in validating the basic body force concept (Figure 2.5) and to calculate the compressor performance using the appropriate body force database (Figure 2.6). More details on the procedure for calculating compressor performance prediction will be presented in Chapter 3.

2.4.1 Procedure for Concept Validation

In the beginning of the process, a Navier-Stokes solver is first used to obtain detailed three-dimensional flow solutions at a mass flow for a given isolated blade row. From the solutions, body forces are extracted by solving the integral form of the momentum equations around the control volumes. The extracted body forces are then substituted as

source terms in an Euler flow solver. For the validation step, an Euler computation is performed with the inflow and outflow boundary conditions used to obtain the Navier-Stokes solutions from which the body forces were extracted.

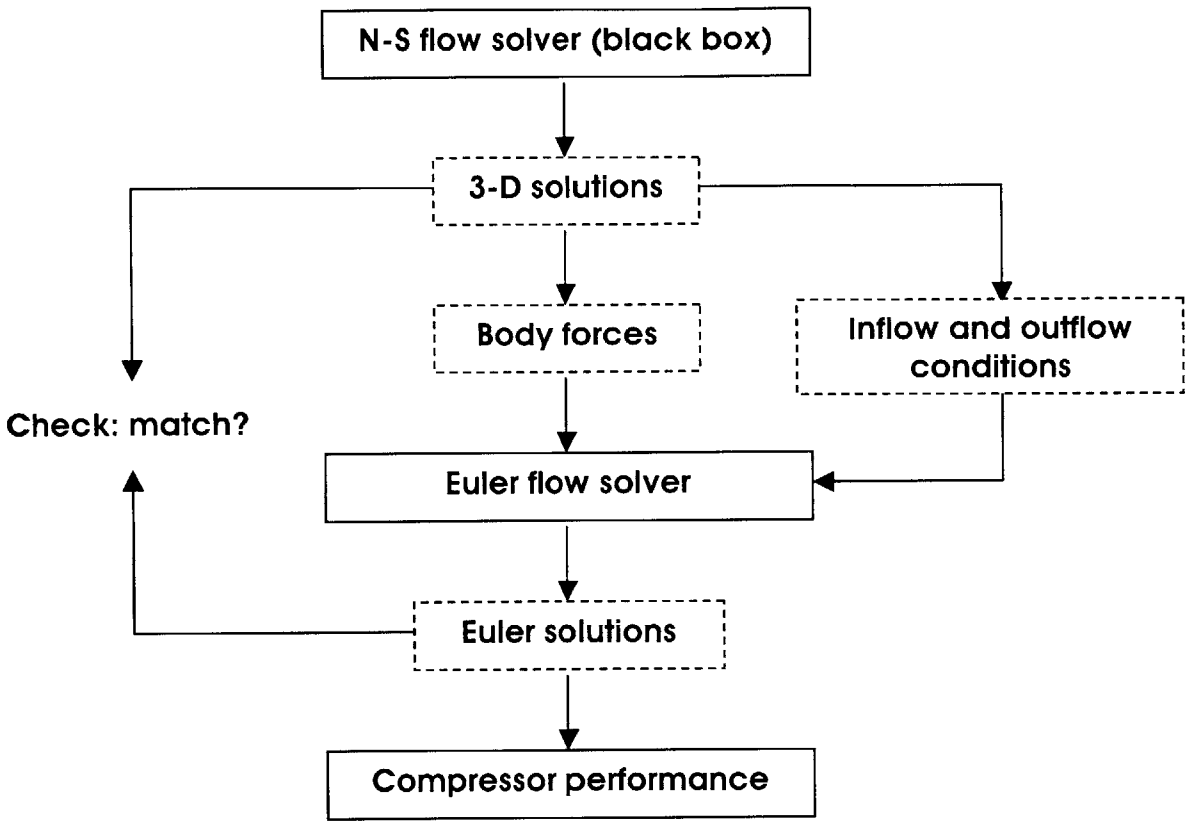

Figure 2.5: Computational methodology for the concept validation

Having obtained the Euler solutions, one- and two-dimensional mass- and area-averaged profiles of flow variables at various cross sections along the axial direction, as well as the compressor pressure rise computed from the Euler solutions, are compared against the Navier-Stokes solutions.

2.4.2 Procedure for Flow Analysis with a Body Force Database

The procedure for practical applications involves two steps. The first step consists of generating a body force database for a given blade row (or a set of blade rows). This step is illustrated graphically in Figure 2.6. A Navier-Stokes solver is first used to compute detailed flow fields at various mass flows on a constant speed-line. From the Navier-Stokes solutions, a body force database is constructed. Once the database is available, no further Navier-Stokes computations are required. This step is performed for each blade row in a multi-stage compressor.

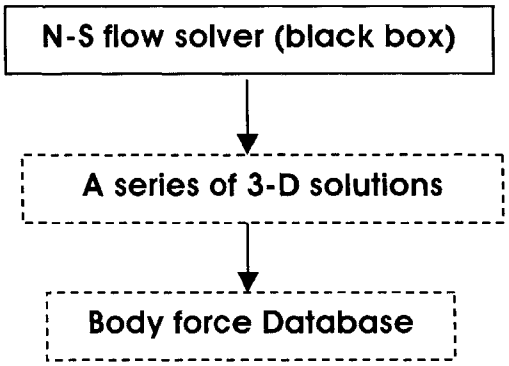

Figure 2.6: Generation of a body force database

Using the body force database, the performance map generation for the compressor under different inflow boundary conditions are carried out using the axi-symmetric Euler solver. Having specified the inflow and outflow boundary conditions of interest in the beginning of a computation, the solver computes the appropriate local flow conditions and residuals at each iteration. If the flow variables converge, the solutions are produced, and the computation is terminated. If not, the local flow conditions are fed into the database to compute correct local body forces and another iteration is performed with the new body forces. This step is repeated until the solution variables converge to a steady

state. Once the converged solutions are produced, the compressor performance is computed.

The whole procedure is repeated with various inflow and outflow boundary conditions and rotating speeds of the rotor blades that are representative for all possible operating conditions until the complete map is obtained.

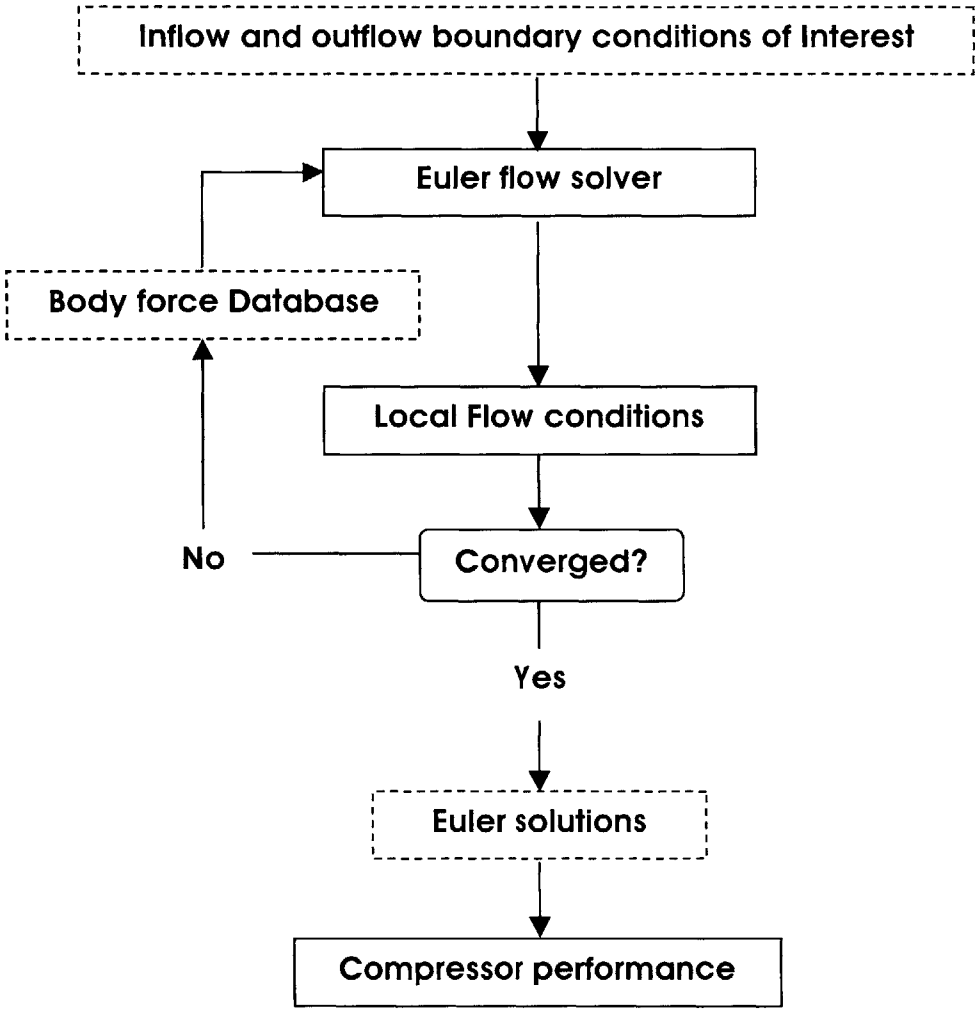

Figure 2.7: Computational procedure for compressor map generation

2.5 Body Force Extraction

This section will describe how a body force field is constructed quantitatively for a given blade row in steady flow at a given operating point. In order to quantify the body forces in the field, it is necessary to know pieces of information about the blade row regarding geometry, operating/boundary conditions, and their corresponding flow field. Depending on the level of accuracy desired, the amount of information required to model the blade row varies.

Hence, a Navier-Stokes code was used in the present work to carry out all necessary computations to obtain the detailed flow information. However, the computational procedure developed here is not tied to a particular Navier-Stokes code. This allows the use of detailed flow solutions from any three-dimensional Navier-Stokes code as long as the solutions are accurate and written in a consistent format.

In this case, for example, all solution vectors produced by the Navier-Stokes computations are assumed to have the PLOT3D format, i.e.

$$\bar{q} = \begin{bmatrix} \rho \\ \rho V_x \\ \rho V_y \\ \rho V_z \\ \rho e \end{bmatrix} \qquad (2.1).$$

In Equation (2.1), $\bar{q}$ is a vector of conservative variables in the Cartesian coordinates in absolute frame of reference, i.e. density, three components of momentum, and total energy per unit volume.

2.5.1 Computing Body Forces

Body forces can be numerically computed once the three-dimensional Navier-Stokes flow variables become available. The current computational methodology requires numerical values of the solution variables at every grid point in the computational domain in order to calculate the body forces.

From the Navier-Stokes solutions, the three components of the body forces per unit mass in cylindrical coordinates, i.e. F_x, F_θ, and F_r are computed. This procedure is implemented by solving the integral form of the momentum equations around the control volumes in the blade row domain. It is noted that, since an axi-symmetric Euler code is used to replace the effects of blades by the body forces, the numerical values of the body forces should also be axi-symmetric in order to be compatible with the code. This implies that the magnitudes of the body forces do not change in the pitch-wise direction.

In general, one of two types of the control volumes can be chosen for the construction of the axi-symmetric body forces: (1) relatively small control volumes surrounded by eight grid points of the original Navier-Stokes domain or (2) larger control volumes that extend from one blade surface to the other in pitch-wise direction at a fixed axial and radial location (see Figure 2.8). The first type of control volume yields body force components with three-dimensional spatial dependence and therefore is exemplary for detailed parametric studies to understand their functional dependence on local flow conditions. However, it requires a mass-averaging technique to obtain axi-symmetric body forces, leading to computational inefficiency. Furthermore, significant numerical errors may arise where the control volumes are extremely small ($\sim 10^{-8}$) because the forces acting on each control volume are obtained by dividing the left hand sides of the momentum equations by the size of the control volume. This type of the control volumes is usually found near the wall boundaries, as well as at the leading and trailing edges of a blade.

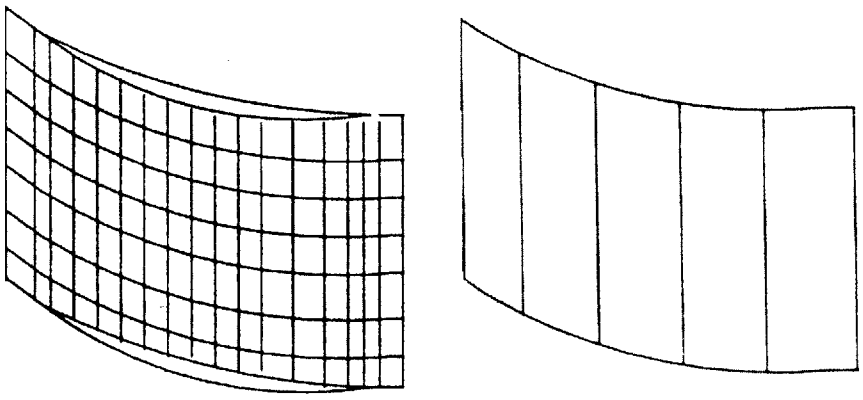

(a) (b)

Figure 2.8: (a) three-dimensional control volumes and (b) axi-symmetric control volumes

The second type of control volume, in contrast, is more efficient in terms of computational time and memory. The numerical errors associated with the control volumes are not expected to be significant with this type due to relatively larger control volumes. Thus, the second type is chosen for the body force extraction. A three-dimensional view of the considered control volumes is depicted in Figure 2.9.

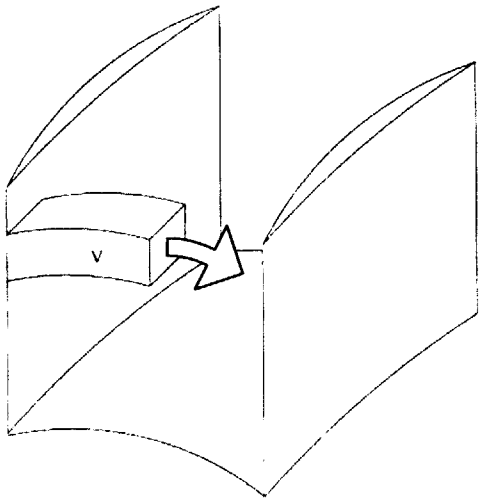

Figure 2.9: Axi-symmetric control volume in a blade row

As the solution variables are provided in Cartesian coordinates, the body forces are first constructed in Cartesian coordinates. The forces can then be converted to the cylindrical components by an appropriate coordinate transformation. Such a transformation is implemented using a rotation matrix. In other words, the Cartesian components of the body forces are first computed by solving the following integral form of the momentum equations

$$\oint_{\partial\Omega} \rho\vec{V}(\vec{V}\cdot\vec{n})dA = -\oint_{\partial\Omega-\Gamma} p\vec{n}dA + \int_{\Omega} \rho\vec{F}_{xyz}dV \tag{2.2}$$

for $\vec{F}_{xyz} = [F_x \quad F_y \quad F_z]^T$, i.e. the body force vector per unit mass in Cartesian coordinates. In Equation (2.2), Ω, $\partial\Omega$, and Γ denote the control volume, control surface, and blade surface, respectively. The cylindrical components are then computed by multiplying the Cartesian components at each control volume by its three-dimensional rotation matrix, as shown in Equation (2.3):

$$\begin{bmatrix} F_x \\ F_\theta \\ F_r \end{bmatrix} = \begin{bmatrix} 1 & 0 & 0 \\ 1 & \cos\theta & -\sin\theta \\ 1 & \sin\theta & \cos\theta \end{bmatrix} \begin{bmatrix} F_x \\ F_y \\ F_z \end{bmatrix} \tag{2.3}$$

where θ is the angle of each control volume at its center with respect to the y-axis plane in Cartesian coordinates. The body force components produced from Equation 2.3 can then be embedded in the new set of governing equations as the source terms.

2.6 Governing Equations

2.6.1 Flow in Ducts

Typically, an inviscid flow in upstream and downstream ducts, and intra-blade-row gaps is described by the three-dimensional compressible inviscid Euler equations. The conservative form of the equations can be written as [8]:

$$\frac{\partial}{\partial t}\begin{bmatrix} r\rho \\ r\rho V_x \\ r\rho V_\theta \\ r\rho V_r \\ r\rho e \end{bmatrix} + \frac{\partial}{\partial x}\begin{bmatrix} r\rho V_x \\ r\rho V_x^2 + rp \\ r\rho V_x V_\theta \\ r\rho V_x V_r \\ rV_x(\rho e + p) \end{bmatrix} + \frac{\partial}{\partial \theta}\begin{bmatrix} \rho V_\theta \\ \rho V_x V_\theta \\ r\rho V_\theta^2 + p \\ \rho V_\theta V_r \\ V_\theta(\rho e + p) \end{bmatrix} + \frac{\partial}{\partial r}\begin{bmatrix} r\rho V_r \\ r\rho V_x V_r \\ r\rho V_\theta V_r \\ r\rho V_r^2 + rp \\ rV_r(\rho e + p) \end{bmatrix} = \begin{bmatrix} 0 \\ 0 \\ -\rho V_\theta V_r \\ \rho V_\theta^2 + \rho \\ 0 \end{bmatrix} \quad (2.4)$$

In the present work, however, all computations using the body force representation are axi-symmetric. This indicates that the terms associated with the variation in the pitch-wise direction can be neglected, i.e.

$$\frac{\partial}{\partial t}\begin{bmatrix} r\rho \\ r\rho V_x \\ r\rho V_\theta \\ r\rho V_r \\ r\rho e \end{bmatrix} + \frac{\partial}{\partial x}\begin{bmatrix} r\rho V_x \\ r\rho V_x^2 + rp \\ r\rho V_x V_\theta \\ r\rho V_x V_r \\ rV_x(\rho e + p) \end{bmatrix} + \frac{\partial}{\partial r}\begin{bmatrix} r\rho V_r \\ r\rho V_x V_r \\ r\rho V_\theta V_r \\ r\rho V_r^2 + rp \\ rV_r(\rho e + p) \end{bmatrix} = \begin{bmatrix} 0 \\ 0 \\ -\rho V_\theta V_r \\ \rho V_\theta^2 + \rho \\ 0 \end{bmatrix} \quad (2.5)$$

2.6.2 Flow in Blade Rows

In a blade row region, the infinite number of blade assumption is made. The assumption implies that the flow is locally axi-symmetric in a coordinate frame fixed to the blade row. The pressure rise and flow turning by the blades can thus be computed by a body

force field. This assumption simplifies the complexity of the model in terms of computational resources.

The governing equations in the absolute frame of reference can be written as:

$$(\frac{\partial}{\partial t}+\Omega\frac{\partial}{\partial \theta})\begin{bmatrix} r\rho \\ r\rho V_x \\ r\rho V_\theta \\ r\rho V_r \\ r\rho e \end{bmatrix}+\frac{\partial}{\partial x}\begin{bmatrix} r\rho V_x \\ r\rho V_x^2+rp \\ r\rho V_x V_\theta \\ r\rho V_x V_r \\ rV_x(\rho e+p) \end{bmatrix}+\frac{\partial}{\partial r}\begin{bmatrix} r\rho V_r \\ r\rho V_x V_r \\ r\rho V_\theta V_r \\ r\rho V_r^2+rp \\ rV_r(\rho e+p) \end{bmatrix}=\begin{bmatrix} 0 \\ r\rho F_x \\ r\rho F_\theta-\rho V_\theta V_r \\ \rho V_\theta^2+\rho+r\rho F_r \\ r\rho(\bar{F}\cdot\bar{V}+\dot{q}) \end{bmatrix} \tag{2.6}$$

where $F_x, F_\theta, F_r, \dot{q}$ are the body force and heat source terms. The units of these terms are force or heat release per unit mass. For the same axi-symmetric argument used in the previous section, Equation (2.6) is simplified to:

$$\frac{\partial}{\partial t}\begin{bmatrix} r\rho \\ r\rho V_x \\ r\rho V_\theta \\ r\rho V_r \\ r\rho e \end{bmatrix}+\frac{\partial}{\partial x}\begin{bmatrix} r\rho V_x \\ r\rho V_x^2+rp \\ r\rho V_x V_\theta \\ r\rho V_x V_r \\ rV_x(\rho e+p) \end{bmatrix}+\frac{\partial}{\partial r}\begin{bmatrix} r\rho V_r \\ r\rho V_x V_r \\ r\rho V_\theta V_r \\ r\rho V_r^2+rp \\ rV_r(\rho e+p) \end{bmatrix}=\begin{bmatrix} o \\ r\rho F_x \\ r\rho F_\theta-\rho V_\theta V_r \\ \rho V_\theta^2+\rho+r\rho F_r \\ r\rho(\bar{F}\cdot\bar{V}+\dot{q}) \end{bmatrix} \tag{2.7}$$

If there is no additional heat source in the fluid, the energy transfer is through the blade force; therefore the source terms in the energy equation is the work done by the rotor blade row. If this is the case, the right-hand side term of the energy equation can be expressed as

$$\bar{F}\cdot\bar{V}+\dot{q}=F_\theta\Omega r \tag{2.8}$$

where Ω is the rotating speed of the blade row, and F_θ is the net pitch-wise body force per unit mass.

2.7 Numerical Method of Solutions

An Euler code initially developed by Gong [8] to simulate axial compressor stall inception was modified to embed the body forces in Equation 2.7 as source terms. In the original version of the code, the body forces are modeled within the code based on overall computed/measured pressure-rise characteristics, whereas in this study, they have been computed by external computer programs and available prior to Euler computations. Those computer programs, developed by the present author, model the body forces utilizing the method described in the previous section. An input file containing the numerical values of the body forces is fed into the code at the start of the computations, along with the files containing grid and inflow and outflow boundary conditions. The boundary conditions are derived from the original Navier-Stokes solutions for the validation cases. The details regarding initial and boundary conditions are provided in Chapter 4.

For the remainder of this section, the numerical methods of the Euler code are described. The solution procedure for solving the nonlinear governing equations is based on a finite volume method in pseudo-time. The pseudo-time terms are approximated by an explicit four-stage Runge-Kutta time-stepping scheme. Inviscid terms are evaluated by using a central differencing scheme. This combination has been shown to yield an effective method for solving the Euler equations in arbitrary geometric domains.

To suppress the tendency for odd and even point decoupling, and to prevent the appearance of wiggles in regions containing severe pressure gradients in the neighborhood of shock waves and stagnation points, the finite volume scheme was augmented by the addition of artificial dissipative terms [12]. An effective form for the dissipative terms was shown to be a blend of second- and fourth-order terms with coefficients that depend on the local pressure gradient. The details of theses methods can be found in [12].

Techniques such as implicit residual smoothing and local time stepping have shown to accelerate convergence to a steady state, but were not implemented by Gong [8] because the code was initially developed for time-accurate unsteady computations.

2.8 Summary

The concepts and basic problem formulations have been covered in this chapter. The purpose of the body force formulation is to replace each blade row in a multi-stage compressor by a body force distribution to produce same pressure rise and flow turning. The new computational methodology developed in the present thesis has a few main advantages over the conventional CFD approaches. They include modeling simplicity and significant reductions in computational costs.

Using the Navier-Stokes solutions, the body forces are first computed in Cartesian coordinates by solving the integral form of the momentum equations, and subsequently transformed to that in cylindrical coordinates by using a rotation matrix. The computed body forces are embedded in the new set of governing equations. The nonlinear equations are solved iteratively by using a standard finite volume method with an explicit four-stage Runge-Kutta time-stepping scheme. Numerical oscillations are suppressed by adding the artificial dissipative terms consisting of second- and fourth-order terms.

CHAPTER 3

DEVELOPMENT OF COMPUTATIONAL METHODOLOGY: PART II

3.1 Generation of Body-Force Database

In Chapter 2, an overview of the computational procedures developed for validation processes and applications was presented. As previously mentioned, the computational procedure for a practical application involves using a body force database constructed from a few isolated blade row Navier-Stokes solutions for the blade row of interest. However, detailed procedural steps associated with the body force database generation were not presented in Chapter 2 so as to provide a concise presentation of the overall computational methodology. Thus, a detailed presentation on the theoretical framework developed for the generation of the database is given in this chapter.

The generation of the body force database is an important part of the current research and thus should not be taken lightly. The theoretical development process made use of a dimensional analysis to determine the local flow conditions by which body forces can be parameterized. The rest of the current section of this chapter is devoted to delineating the detailed steps and analysis involved in the procedure.

In this chapter, the main objectives are (1) to cover the detailed steps involved to generate the body-force database, (2) to identify the local flow conditions which can be employed to parameterize the forces, and finally (3) to identify applications. The successful

accomplishment of these objectives listed above will finalize the presentation on the development of the computational methodology.

3.1.1 Parametric Representation of Body Forces

Computing compressor performance for a new operating point is achievable if the body forces are capable of responding to the changes in the inflow and outflow boundary as well as the operating conditions. The changes in the inflow and outflow boundary conditions include, for example, perturbations in the radial total pressure, total temperature, axial, and/or tangential velocity profiles in the upstream region, and/or usually exit static pressure profile in the downstream region of the blade row.

Since those changes usually dictate the changes in the local flow conditions in the blade row, one of the main goal of the parameterization is to enable the body-forces to respond to the changes in the local flow conditions rather than the boundary or operating conditions. To determine what those local flow conditions are, a dimensional analysis using the Π-Theorem [7], [24] is implemented.

3.1.1.1 Dimensional Analysis

The first part of the dimensional analysis consists of identifying all the possible independent variables in the governing equations of interest. In this case, the governing equations of interest are the Navier-Stokes equations. Assuming the body forces can be written in terms of some unknown functions of the independent variables of the Navier-Stokes equations in cylindrical coordinates in the relative frame, the following three equations can be obtained:

$$\begin{aligned} F_x &= f_z(\rho,[V_x]_R,[V_r]_R,[V_\theta]_R,p,\mu,r) \\ F_\theta &= f_\theta(\rho,[V_x]_R,[V_r]_R,[V_\theta]_R,p,\mu,r) \\ F_r &= f_r(\rho,[V_x]_R,[V_r]_R,[V_\theta]_R,p,\mu,r) \end{aligned} \qquad (3.1)$$

where in the left hand side, F_x, F_θ, and F_r denote the axial, tangential, and radial forces per unit mass, respectively. The physical quantities in the right hand side are the independent variables in the governing equations. Namely, they are density, three velocity components, static pressure, dynamic viscosity, and the radius (or any other appropriate characteristic length of the blade), respectively. The subscript R in Equations 3.1 denotes the relative frame of reference.

Since Equation 3.1 share the common variables, they can be written in terms of a vector form by first defining the body-force vector as follows:

$$\vec{F} = \begin{bmatrix} F_x & F_\theta & F_r \end{bmatrix}^T \tag{3.2}.$$

Using Equation 3.2, Equations 3.1 can be rewritten as

$$\vec{F} = \vec{f}(\rho, V_x, V_r, V_\theta, p, \mu, r) \tag{3.3}$$

Applying the Π-Theorem to Equation 3.3 produces the following functional relationship:

$$\frac{r\vec{F}}{U_R^2} = \vec{f}(\alpha_r, \alpha_\theta, M_R, Re_R) \tag{3.4}$$

where U_R is the magnitude of the local relative velocity. Equation 3.4 implies that the non-dimensional form of the body forces is a function of the following dimensionless variables: relative radial and tangential flow angle, relative Mach number, and the Reynolds number.

3.1.1.2 Subsonic Flows

In general, the relative flow angles in Equation 3.4 should always be considered for the subsonic flow regime: conceptually, the body forces are proportional to the relative flow

angles. This statement is also supported by Gong's work [8]. If the compressibility effect is significant, the relative Mach number should also be included to reflect the effect, in addition to the relative flow angles. In other words, the functional form now becomes

$$\frac{r\vec{F}}{U_R^2} = \vec{f}(\alpha_r, \alpha_\theta, M_R) \tag{3.5}$$

If the Reynolds number is considerably low, then the Reynolds number must be included as well, i.e.

$$\frac{r\vec{F}}{U_R^2} = \vec{f}(\alpha_r, \alpha_\theta, M_R, Re_R) \tag{3.6}$$

3.1.1.3 Supersonic Flows

For supersonic flows, however, it was found that the relative flow angles could be neglected: the shock waves within the blade passage determine and fix the downstream flow angles. Given the inflow and metal angles, the downstream flow angles can be analytically estimated by using the shock theory found in any gas dynamics textbook. The computed local flow angles from the Navier-Stokes solutions in this flow regime show that their magnitudes do not change at all, although the body forces change noticeably. Therefore, it is concluded that for the supersonic flows, the non-dimensional form of the body forces can be parameterized as:

$$\frac{r\vec{F}}{U_R^2} = \vec{f}(M_R) \tag{3.7}$$

For the high Reynolds number flow considered here, the Reynolds number dependence can be neglected. That is, the only local flow condition required to parameterize the body forces is the local relative Mach number. As high-speed (transonic) blade rows are being considered here, Equation 3.7 is used for the parameterization.

3.1.2 Generation Procedure

Having identified the local relative Mach number as the sole local flow quantity by which the magnitudes of the body forces at each point in the blade row region can be estimated in the supersonic flow regime, a general procedure adapted to generate a consistent body-force database will be demonstrated here.

To generate the database, several Navier-Stokes solutions of a blade row for various mass flows on a constant speed-line are required in order to estimate the governing relationships between the relative Mach number and the body forces. The solutions from at least two different mass flows are necessary to generate the database. However, the corresponding database will be low-order accurate, since it is impossible to correctly predict any non-linear behavior with only two operating points. Therefore, solutions obtained from more than two operating points are recommended.

To estimate the body force components between any two points along the speed-line, an interpolation scheme was employed. For the current applications, the linear interpolation was used. Figure 3.1 shows how the database is organized at each cell in the blade row.

3.2 Potential Engineering Applications

In this section, important potential engineering applications using the computational methodology with the body-force database other than compressor map generation are discussed.

3.2.1 Response to Radial Inlet Distortions

The first useful engineering application is a performance prediction of a rotor subjected to radial inlet distortions. The graphical demonstration in Figure 3.2 shows how the

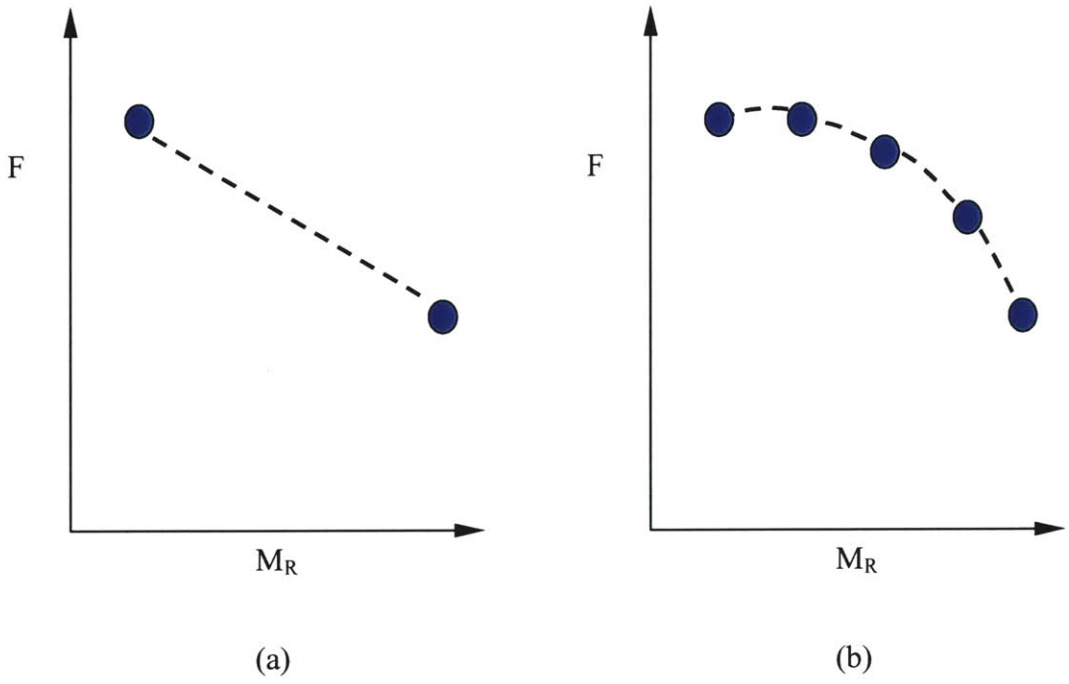

Figure 3.1: An example of the body-force database organization at each local point: (a) database generated from Navier-Stokes solutions at two operating point. Non-linear dependence cannot be captured. (b) database generated from solutions at more than two operating points. In this situation, the non-linear behavior can be well captured.

prediction can be carried out: in this example, Navier-Stokes solutions obtained at three mass flows, for example, with different uniform inflow conditions, denoted as 1, 2, and 3, were used to generate a body force database. Assuming that point 1, 2, and 3 cover a broad range of mass flows on a speed-line, the resulting database should be able to predict the new compressor performance subjected to non-uniform radial profiles, such as the one shown in Figure 3.2.

3.2.2 Performance of a Multi-Stage Compressor

The second important application is a performance prediction of a multi-stage compressor using the body force approach. The body force database for each blade row is obtained from the solutions of isolated blade row computations (and not from multi-stage computations) for that blade row. In other words, independent Navier-Stokes computations are performed for each isolated blade row at various mass flows. For the isolated blade row Navier-Stokes computations, each blade row is completely uncoupled and does not interact with its neighboring blade(s), whereas for the multi-stage computation, each blade row is coupled with its neighboring blade rows by interactions at the boundary interfaces.

Conceptually, this is a direct extension of the concept shown in the first application. The reason is that a downstream blade row in the multi-stage compressor experiences non-uniform inflow conditions generated by the presence of its upstream blade row propagating into the blade row. This is depicted in Figure 3.3.

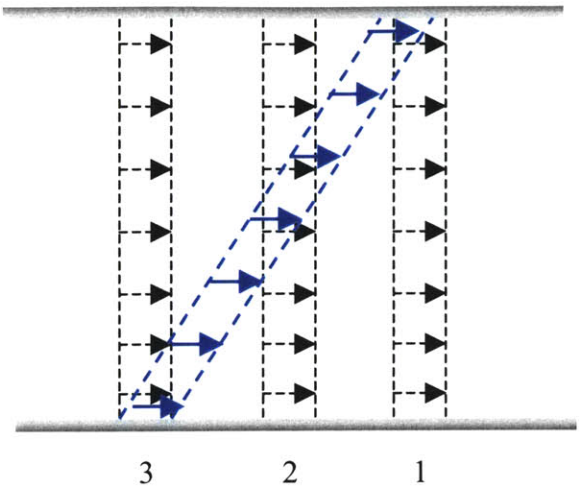

Figure 3.2: Utilization of body-force database for non-uniform inlet conditions

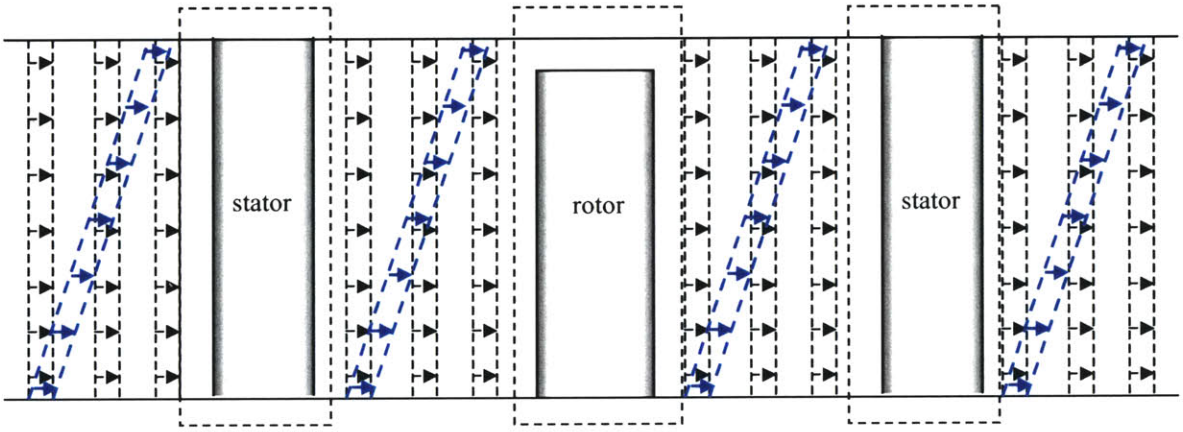

Figure 3.3: Utilization of body-force databases for a multi-stage configuration

3.3 Summary

A dimensional analysis using the Π-Theorem was carried out to determine the local flow conditions that govern the magnitudes of body forces. The followings were inferred from the results of the analysis: the non-dimensional form of the body forces can be parameterized in terms of (1) the two relative flow angles, and Reynolds number for low Reynolds number flows in the subsonic flow regime; (2) the two relative flow angles and relative Mach number if the compressibility effect becomes significant for flows in the subsonic flow regime; and (3) only relative Mach number for flows in the supersonic flow regime.

To generate a body-force database, several Navier-Stokes solutions are required. Solutions obtained from at least two operating points are necessary, but using more solutions is recommended for higher accuracy.

Useful engineering applications using the computational methodology developed in Chapters 2 and 3 include a performance prediction of a single rotor blade row subjected to radial inlet distortions and a prediction of the accurate continuous flow field in a multi-stage compressor.

CHAPTER 4

DESCRIPTION OF TEST CASES

4.1 Introduction

This chapter describes all the test cases that were considered during the course of the current research in order to validate the computational methodology developed in Chapters 2 and 3. For each test case, detailed descriptions of the investigated blade row, grid dimensions of both Navier-Stokes and Euler computations performed, and operating conditions under which the test case was carried out are presented.

There were a total of four test cases conducted in the current work. The first three test cases made use of the NASA Rotor 37, a high-speed single rotor blade row for an advanced high-pressure-ratio core compressor. This single-stage compressor was an ideal candidate for the first three test cases to validate the methodology because of the availability of its extensive experimental and computational data to the public domain [20]. The fourth test case consisted of the IGV-rotor-stator configuration of a high-pressure compressor that had a high bypass ratio representative of a modern design.

The rest of this chapter is devoted to presenting and describing the details of these test cases. All the corresponding computational results from the test cases and their comparisons against the Navier-Stokes solutions are given in Chapter 5.

4.1.1 More Details on NASA Rotor 37

The NASA Rotor 37 is a high-speed research compressor with a high-pressure ratio. It was developed and tested by the NASA in late 1970s as a part of their research program on evaluating the overall performance characteristics of four single stages, i.e. Rotors 35, 36, 37, and 38, that are representative of inlet, middle, and rear stages of an eight-stage 20:1 pressure ratio core compressor.

The rotor has an aspect ratio of 1.19, with an inlet hub-tip ratio of 0.7. It was designed for a total pressure ratio of 2.106 at a mass flow of 20.20 kilograms per second, with the inlet rotor-tip speed of 455 meters per second. In experimental test at design speed, however, the total pressure ratio across the rotor was determined to be 2.056, with an efficiency of 0.876, and actual mass flow rate of 20.74 kilograms per second.

The original configuration of the experimental hardware testing performed by the NASA was a single-stage compressor consisting of a rotor blade row followed by a stator blade row. However, in the current work, the stator blade row was not computationally modeled.

4.2 Test Case 1: Validation on Applicability of Model

The NASA Rotor 37 was chosen for the first three test cases to demonstrate the capability of the computational methodology developed in the previous two chapters (1) to replicate a flow field from which the body forces are extracted, (2) to respond to non-uniform radial inlet distortions using a body force representation that responds to local flow conditions, and (3) to predict the compressor performance at a completely new operating point, of which mass flow is located within the range of the body force database.

For the first case presented in this section, body forces in the blade row region were not redistributed in response to the changes in the local flow condition. In other words, the body forces were extracted from the Navier-Stokes solutions at one operating point at the design speed and directly substituted in the blade row region in an Euler computation to reproduce the same flow field by matching the mass flow.

The main goal of the test case was simply to illustrate that the body forces can be substituted for the effects of the blade row. The redistribution capability of the body forces was examined in the latter test cases.

4.2.1 Description of Navier-Stokes Solutions

To construct the body forces in the blade row, steady state Navier-Stokes solutions that correspond to 98% design mass flow of the compressor and its grid domain were obtained. The Navier-Stokes solutions were post-processed first to determine the operating and boundary conditions and to understand the overall flow characteristics of the compressor. The boundary conditions obtained were then used for the Euler computations performed later in the process. These same pre-processing steps were taken for all the latter test cases as well.

The grid system for the Navier-Stokes solutions had 165 x 36 x 62 grid points in the x-, θ-, and r-directions, respectively. This is equivalent to 368,280 points. Figure 4.1 shows that a considerable number of the grid points were clustered near the leading and trailing edges of the blade, the end-wall boundaries, and the tip clearance region to correctly capture the detailed three-dimensional flow features. The grid points were also finely clustered near the wall boundary surfaces of the blade for resolving the boundary layers adequately. This clustered grid point can be seen in Figure 4.2.

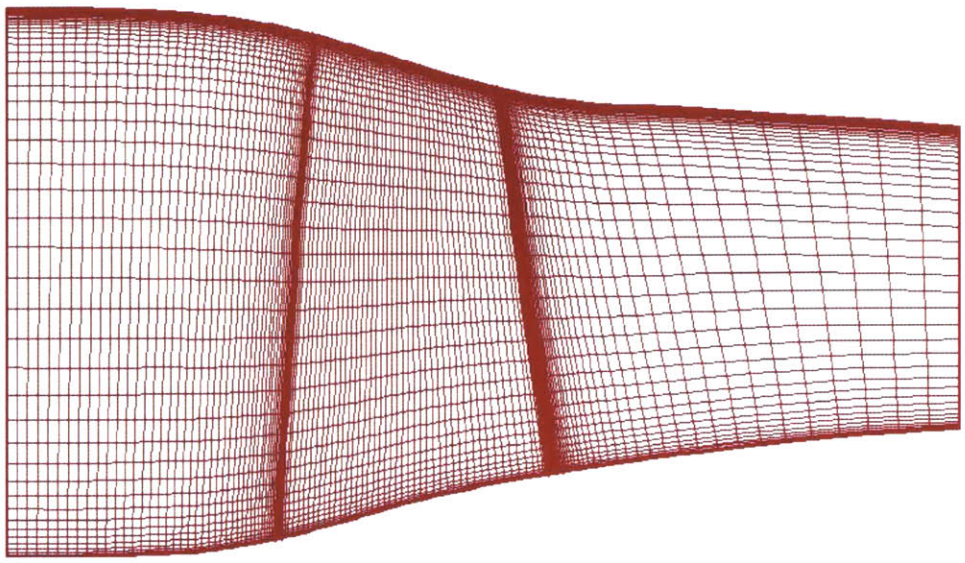

Figure 4.1: Two-dimensional view (x-r plane) of the Navier-Stokes grid system

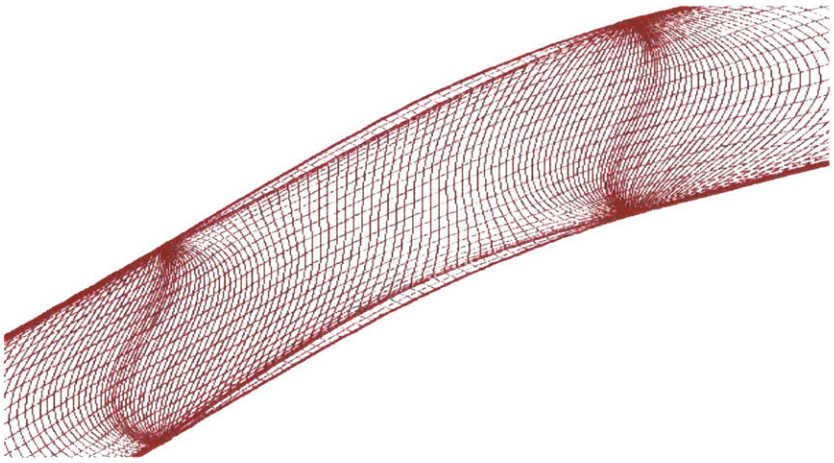

Figure 4.2: x-θ plane of the Navier-Stokes grid system at a constant radial location near the mid span

The flow solutions were provided in the conventional PLOT3D multi-block format. However, the solution variables in this case were non-dimensionalized by their free-stream average flow quantities as follows:

$$\vec{q}' = \begin{bmatrix} \rho' \\ (\rho V_x)' \\ (\rho V_y)' \\ (\rho V_z)' \\ (\rho e_t)' \end{bmatrix} = \begin{bmatrix} \frac{\rho}{\rho_{avg}} \\ \frac{\rho V_x}{\rho_{avg} U_{avg}} \\ \frac{\rho V_y}{\rho_{avg} U_{avg}} \\ \frac{\rho V_z}{\rho_{avg} U_{avg}} \\ \frac{\rho e_t}{\rho_{avg} U_{avg}^2} \end{bmatrix} \tag{4.1}$$

where the variables with the prime denote the non-dimensional variables. The non-dimensionalizing quantities, ρ_{avg} and U_{avg}, represent the average density and velocity magnitude, respectively. For this case, they are

$$\rho_{avg} = 2.11822 \times 10^{-3} \ \frac{slug}{ft^3} \tag{4.2}$$

$$U_{avg} = 544.4734 \ \frac{ft}{sec} \tag{4.3}.$$

In Equation 4.1, the magnitudes of the non-dimensional velocities were provided with respect to the relative frame of reference. Assuming that the x-direction of the computational domain is aligned with the axial flow direction of the compressor, and the rotor blade row rotates in the negative θ-direction, the velocity components with respect to the absolute frame of reference can be obtained by using the following relations:

$$(V_x)_{absolute} = (V_x)_{relative} \tag{4.4}$$

$$(V_y)_{absolute} = (V_y)_{relative} - z\omega \tag{4.5}$$

$$(V_z)_{absolute} = (V_z)_{relative} + y\omega \tag{4.6}$$

where y and z are the y- and z-coordinates of each grid point from the center of rotation, respectively. The symbol ω represents the rotating speed, and for this case, it was:

$$\omega = 17188.7 \frac{\text{rev}}{\text{min}} = 1800 \frac{\text{rad}}{\text{sec}} \qquad (4.7).$$

which is the design wheel speed.

4.2.2 Description of Euler Computation with Body Forces

Instead of generating a completely new Euler grid system, the Euler grid generation was obtained simply by removing the grid points from highly-clustered regions in the Navier-Stokes grid domain. Mainly, the clustered grid points near the wall boundaries as well as in the tip clearance region were removed. This removal process significantly reduced the number of grid points both in the axial and radial directions. Furthermore, since there are no blade geometries present in the computational domain, only two grid points were used in the circumferential direction.

As a result, the new Euler grid system had 68 x 2 x 25 grid points in the x-, θ-, and r-directions, respectively, which is equivalent to 3400 grid points. A noticeable reduction in the total number of grid points is clearly visible. Figure 4.3 shows a two-dimensional view (x-r plane) of the Euler grid system that was produced and adopted for this test case.

All inflow and outflow boundary conditions used for the Euler computation were constructed from the Navier-Stokes solutions. Since the Euler computation was axi-symmetric, the three-dimensional flow solution variables were mass-averaged in the pitch-wise direction, except the axial velocity and the static pressure, for which the area-averaging technique was employed.

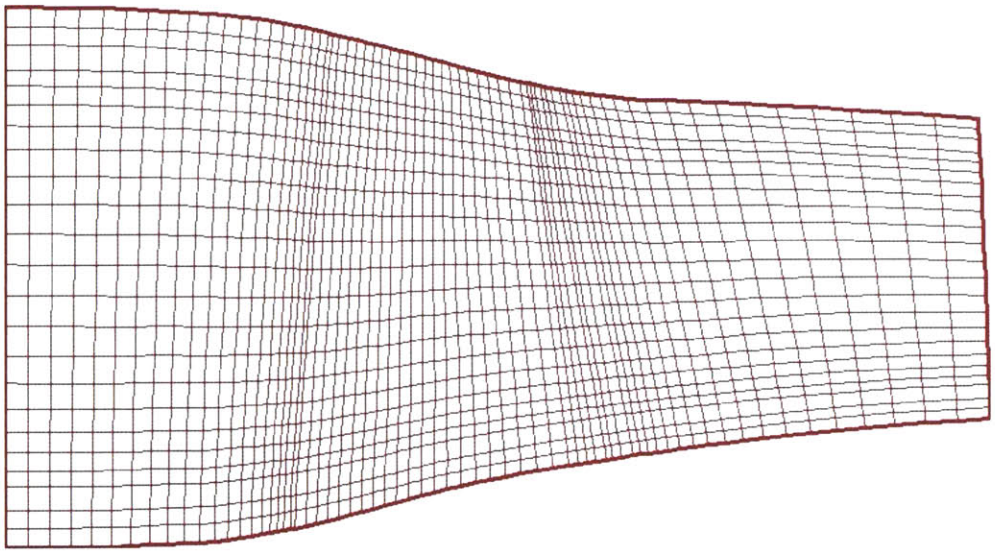

Figure 4.3: Two-dimensional view of the Euler grid system used

4.3 Test Case 2: Redistribution of Body Forces

The main purpose of the second test case was to assess the applicability of local relative Mach number as the single parametric variable to redistribute the body forces acting in the blade row region when the flow relative to the blade is supersonic. As mentioned previously, the NASA Rotor 37 was also used for the current test case. Multiple Navier-Stokes solution files, which represent the compressor performance characteristics on a constant speed-line, were necessary to generate a body force database with a parametric dependence on the local relative Mach number. This database was read in as an input for the Euler code to compute appropriate magnitudes of the body forces once the local relative Mach number was computed at each iteration level.

4.3.1 Description of Navier-Stokes Solutions

The grid system provided for the NASA Rotor 37 with the solution files for the second test case had distinct grid point distributions, as shown in Figure 4.4. The new Navier-Stokes grid system had two less grid points in the axial direction, i.e. 163 x 36 x 62 grid points in x-, θ-, and r-directions, respectively. Furthermore, a significant number of grid points were clustered near the inflow boundary. These changes in the grid system required a new Euler grid generation to embed the body forces consistently in the blade row region. Details about the new Euler grid are provided in the next sub-section.

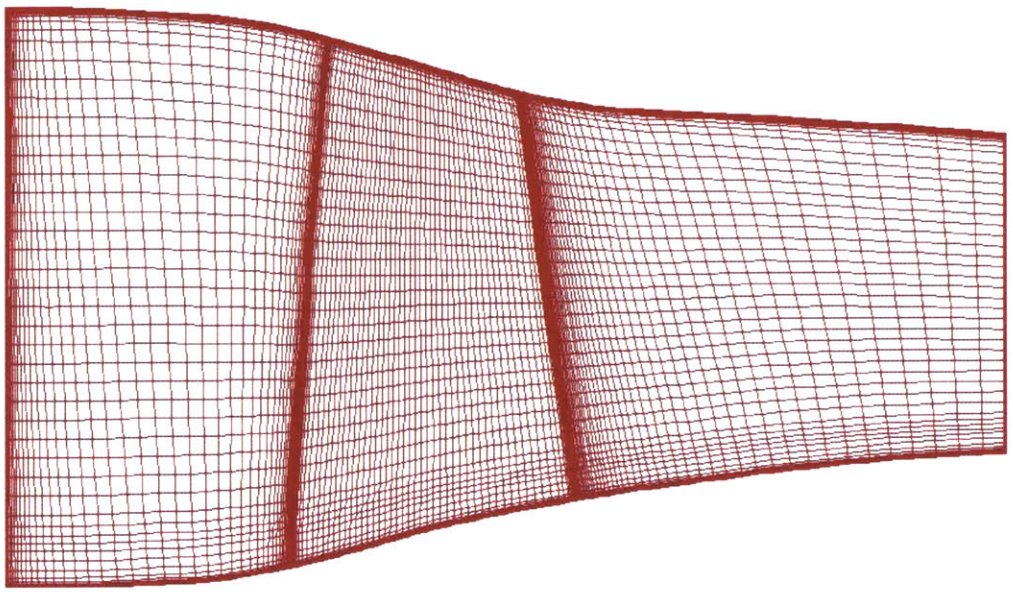

Figure 4.4: Two-dimensional representation of the Navier-Stokes solutions for test case 2

Six Navier-Stokes solutions were provided for this test case. They represent the performance characteristics of the compressor at various mass flows on the design speed-line, which is 17188.7 rpm. The six mass flows are as follows: 42.70 lbm/s, 43.24 lbm/s,

44.16 lbm/s, 45.20 lbm/s, 45.77 lbm/s, and 46.00 lbm/s. Figure 4.5 shows the pressure-rise characteristics computed from the six solution files.

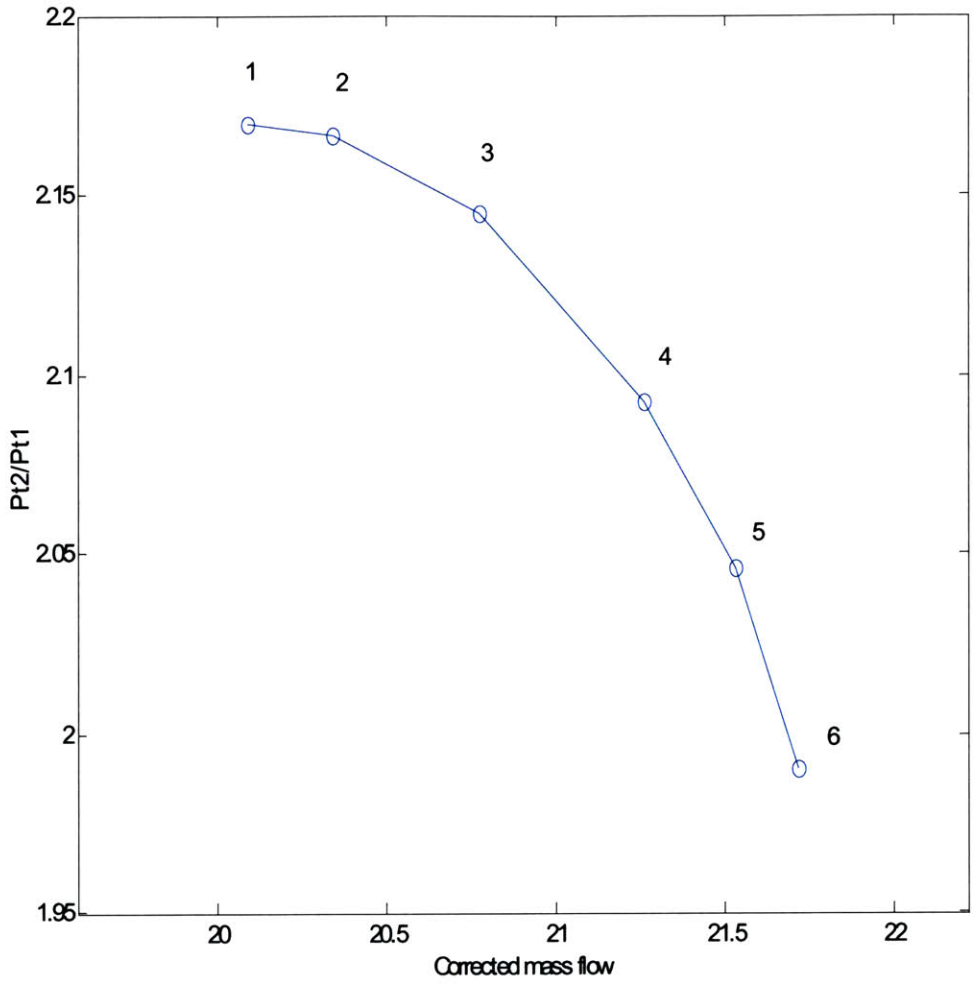

Figure 4.5: Pressure-rise characteristic curve of NASA Rotor 37 on its design speed-line

However, only the flow solutions at three mass flows were selected to construct a simple body force database for the validation purpose: the solutions at the mass flows 44.16 lbm/sec, 45.20 lbm/sec, and 45.77 lbm/sec (operating points 3, 4, and 5 in Figure 4.5) were chosen because they represent a range of the mass flows near the design point.

The new solution files contained the flow variables in the traditional PLOT3D multi-block format, i.e.

$$\vec{q} = \begin{bmatrix} \rho \\ \rho V_x \\ \rho V_y \\ \rho V_z \\ \rho e \end{bmatrix} \tag{4.8}$$

As in the first test case, the velocity components shown in Equation 4.8 were in the relative frame of reference. Therefore, the coordinate transformation techniques elaborated in Section 4.2.1 were employed to obtain the velocity components in the absolute frame of reference.

4.3.2 Description of Euler Computation with Body Forces Database

The new Euler grid system was also generated simply by removing grid points from the Navier-Stokes grid system. The grid removal methodology, explained in Section 4.2 was adopted to remove the grid points. In addition to the current methodology, the clustered grid points near the inflow boundary were removed. As a result, the new Euler grid system had 74 x 2 x 30 grid points in the x-, θ-, and r-directions, respectively. This is equivalent to 4440 grid points. The new Euler grid is shown in Figure 4.6

Using the body force database for this rotor blade row, an Euler computation was carried out to reproduce the pressure-rise characteristic of the compressor at one of the mass flows from which the body force database was created. The middle operating point, i.e. 45.20 lbm/sec (point 4 in Figure 4.5) was chosen to replicate, using the inflow and outflow boundary conditions obtained from the Navier-Stokes solutions for this operating point. If the formulation and all the intermediate steps taken to carry out the Euler computation are consistent, the axi-symmetric flow field and the pressure-rise

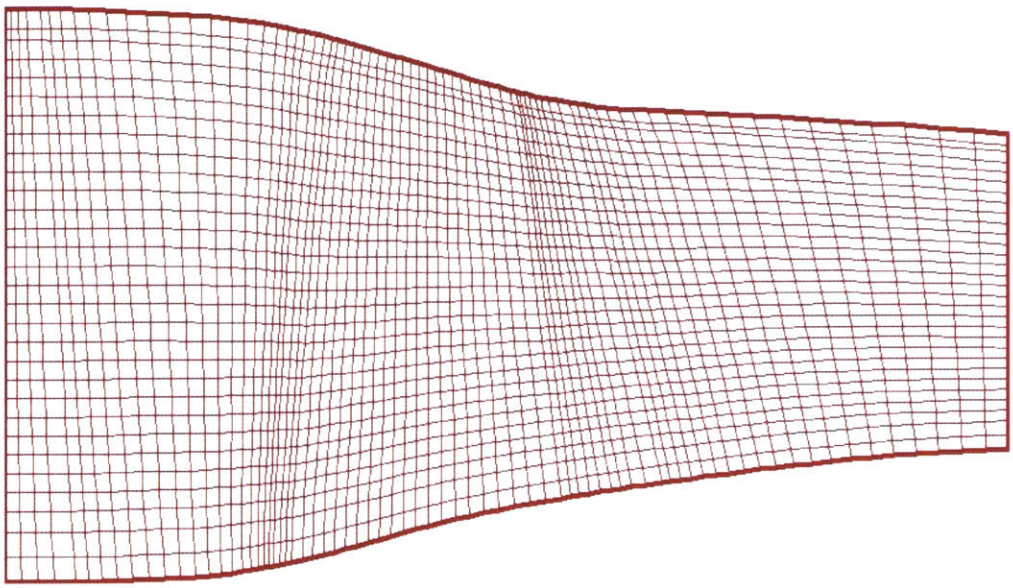

Figure 4.6: Two-dimensional representation of the Euler grid system used for assessing the applicability of the body force redistribution

characteristic of the compressor computed using the database should be exactly the same as from the Navier-Stokes solutions.

4.4 Test Case 3: Radial Inlet Distortions

Having carried out the validation test cases shown in the two previous sections, the main goal of the third test case was to assess the capability of the body force database for predicting the correct compressor performance subjected to radial inlet distortions. The blade row with the radial inlet distortions considered in this test case essentially represents a blade row in a multi-stage compressor. The same database, created from the Navier-Stokes solutions representing the three operating points with uniform inflow boundary conditions, was used for this test case.

4.4.1 Description of Navier-Stokes Solutions

Navier-Stokes solutions for the NASA Rotor 37 using the non-uniform radial inlet total pressure profile shown in Figure 4.7 were provided. The Navier-Stokes grid system for the solutions was identical to the one in the second test case. The variation of the total pressure near the casing at the inlet boundary is about 3.3% with respect to the mass-averaged total pressure value at the inlet, computed from the three solution files that were used to create the body force database. In terms of non-dimensional quantities, the total pressure variation is

$$\frac{\Delta P_t}{\left(\frac{1}{2}\rho V^2\right)_{inlet}} \approx 0.25 \qquad (4.9)$$

The variation of the non-uniform radial inlet total pressure profile had resulted in a linear variation in the axial velocity radial profile, shown in Figure 4.8. The variation in the axial velocity was found to be within the range of the area-averaged axial velocities for the mass flows from which the body force database was constructed.

4.4.2 Description of Euler Computation

The same Euler grid system described in Section 4.3.2 was also used for this test case. The Euler computation was performed by using the body force database constructed from the second test case, and only the boundary conditions were extracted from the Navier-Stokes solutions for the radial inlet distortions. However, the converged solutions from the Euler computation were compared against the Navier-Stokes solutions. The results and comparisons are presented in Chapter 5.

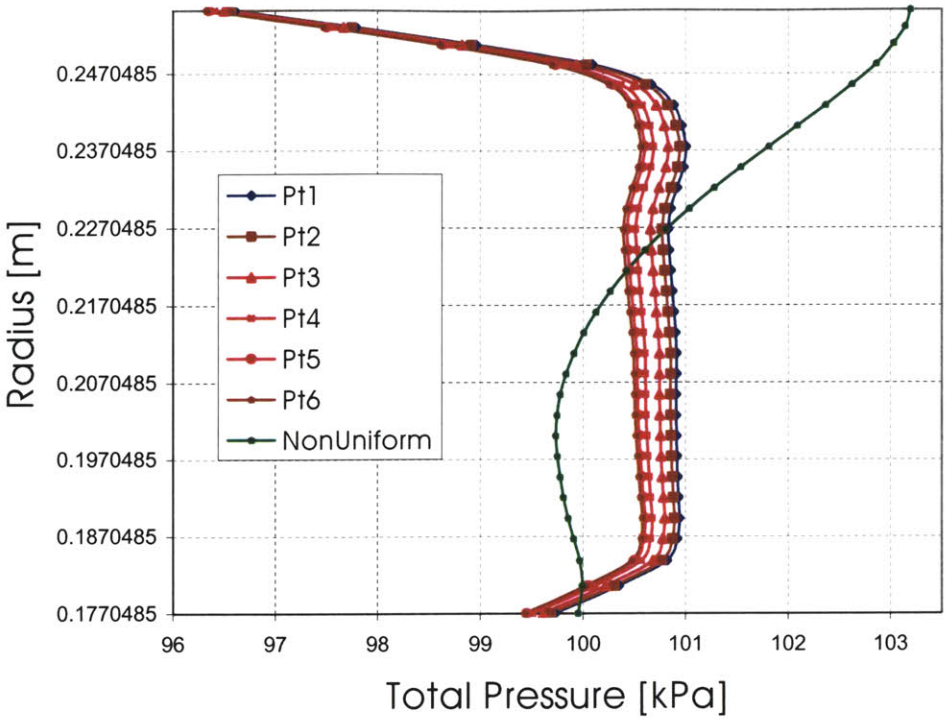

Figure 4.7: Comparisons of the inlet total pressure profiles

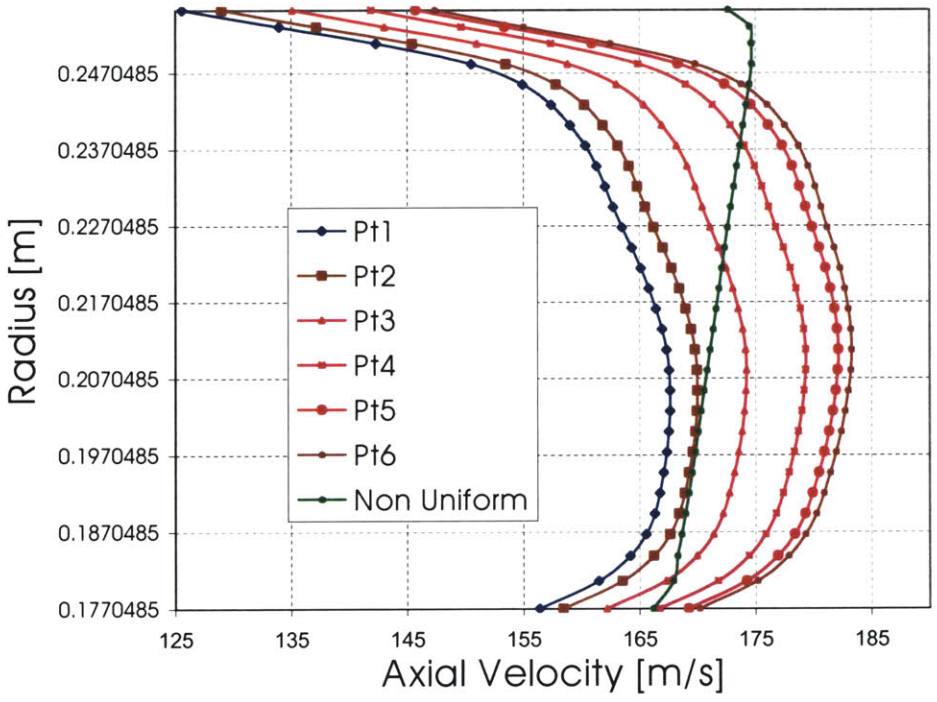

Figure 4.8: Comparisons of inlet axial velocity profiles

4.5 Test Case 4: IGV-Rotor-Stator Configuration

The last test case consists of performing an Euler computation using a body force database for the IGV-rotor-stator configuration of a high-pressure compressor with a high bypass ratio. The purpose of this test case is to assess the applicability of the body force concept validated in the first three test cases on the single blade row for multi-stage flow analysis.

Here, the main idea is to construct a continuous flow field across the compressor with the extracted body forces in the multi-stage environment. The body forces are constructed from isolated blade row Navier-Stokes solutions with essentially uniform inflow conditions for each blade row. The new multi-stage flow solutions are then compared against the multi-blade row Navier-Stokes solutions.

4.5.1 Description of Isolated-Blade Row Navier-Stokes Solutions

For each blade row, Navier-Stokes solutions at three different mass flows, i.e. 321 lbm/s, 325 lbm/s, and 328 lbm/s, were obtained for the IGV-rotor-stator configuration described previously. Thus, a total of nine solution files were used. The rotating speed of the intermediate rotor blade row was computed from the solutions provided in the relative frame of reference and was found to be 10038.31 rpm, which is equivalent to 1051.21 rad/sec. This speed is assumed to be the design speed for the high-speed compressor.

The computational grid systems used for the multi-stage configuration are shown with a distinct color for each flow domain in Figure 4.9. Clearly, a separate grid domain was used for each isolated blade row. The grid dimensions for each blade row are shown in Table 4.1. All three domains had identical indices for the leading and trailing edges in the axial direction and for the tip in the radial direction. This common feature among the

blade rows allowed the body force to be extracted rather conveniently, using the same input file for the computer program with a minimal modification.

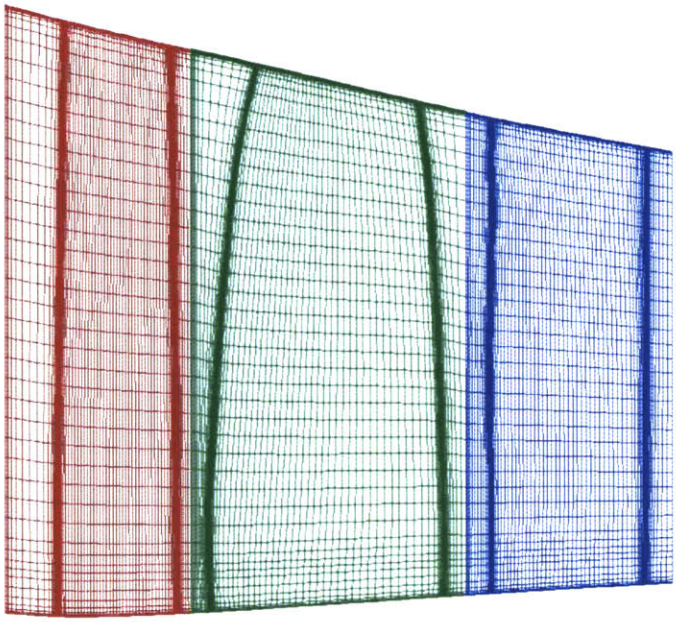

Figure 4.9: Two-dimensional view of the IGV-rotor-stator configuration of HPC for Navier-Stokes solutions

Domain	I-direction	J-direction	K-direction
IGV	96	36	62
Rotor	96	36	62
Stator	96	36	62

Table 4.1: Navier-Stokes grid systems for the multi-stage configuration

4.5.2 Description of Multi-Blade Row Navier-Stokes Solutions

Multi-blade row Navier-Stokes solutions were obtained mainly for the validation purpose, all at the same mass flows specified in Section 4.5.1. The inflow and outflow boundary conditions used for the corresponding Euler computation were constructed from those solutions with identical boundary conditions: the inflow boundary conditions from the IGV solutions and the outflow boundary condition from the stator solutions. The rotating speed of the rotor blade row was computed to be the same as in the isolated blade row solutions.

The grid systems for the multi-blade solutions showed that extra phantom cells were used to mimic the effects of adjacent blade rows. Detail computational and modeling methodologies used in conjunction with the phantom cells were not provided, however. The presence of the phantom cells in each grid domain made the dimensions of the grid system larger in the axial direction. Nevertheless, the grid dimensions were reduced to the original dimensions once the cells were removed.

4.5.3 Description of Euler Computation

As in the previous three test cases, coarsening the Navier-Stokes grid systems to obtain a suitable Euler grid system for the test case was performed in the similar fashion. However, this process produced a diverse set of grid dimensions for each domain due to spatial variations in grid distributions. Table 4.2 shows the dimensions of the new Euler grid system.

The Euler grid systems were then joined together to form a complete grid domain for the entire configuration. The axial dimension of the complete grid system is also shown in Table 4.2. Since two axial planes among the three domains coincided, the computational domain for the entire configuration had two lesser grid points in the axial direction. The two-dimensional representation of the entire domain is shown in Figure 4.10.

Domain	I-direction	J-direction	K-direction
IGV	28	2	32
Rotor	31	2	32
Stator	33	2	32
Complete	90	2	32

Table 4.2: Euler grid systems for the multi-stage configuration

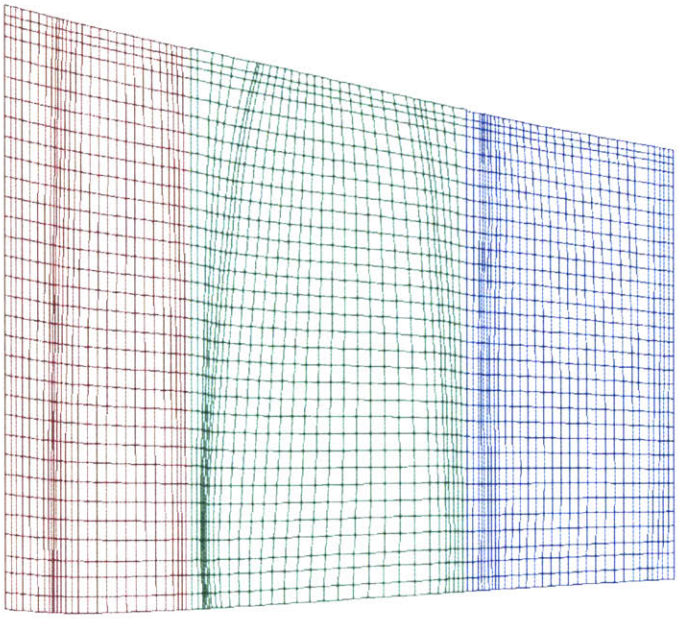

Figure 4.10: Two-dimensional view of IGV-rotor-stator configuration for the Euler computation

The middle operating point, i.e. 325 lbm/s was chosen for the validation. Thus, inflow and outflow boundary conditions constructed from the multi-blade row Navier-Stokes solutions for this operating point were used.

4.6 Summary

Four test cases considered to validate the computational methodology developed in Chapter 2 and 3 were described in this chapter. The first three test cases made use of the NASA Rotor 37, an ideal candidate to validate the methodology because of the availability of its extensive experimental and computational data to the public domain. The last test case consisted of an IGV-rotor-stator configuration of a high-pressure compressor with a high bypass ratio. For each test case, detailed descriptions of the investigated blade row, grid dimensions of both Navier-Stokes and Euler computations performed, and operating conditions under which the test case was carried out were presented. All the corresponding computational results from the test cases and their comparisons against the Navier-Stokes solutions are given in Chapter 5.

CHAPTER 5

RESULTS AND DISCUSSIONS

5.1 Test Case 1: Validation of Basic Model

The Navier-Stokes solutions obtained for this test case were first post-processed to delineate the flow features and determine the operating conditions. The information obtained from this post-processing step was then used for the Euler computations to be implemented subsequently. The body forces for representing a high-speed blade row with high performance should be modeled and extracted on a consistent basis; this is needed to enable an Euler solver with the body force representation of a blade row to yield solutions that match the Navier-Stokes solutions. The next several sub-sections are devoted to explain how carefully the body forces are modeled and extracted, and results obtained by using such body forces are presented.

5.1.1 Generation of Body-Force Grid System

The grid points from the original Navier-Stokes grid system were highly clustered near the wall boundaries. Also, the grid points in an I-index did not have a constant x-value, making it difficult to extract the body forces in the blade row region directly from the solutions obtained with the original grid system. Therefore, the generation of a new body force grid system was needed to extract the body forces from the given Navier-Stokes solutions. During the new grid generation process, the grid points from the original grid

system were evenly re-distributed in the pitchwise direction and were aligned so that the grid points in the I-index have the constant x-value in the axial direction. The original Navier-Stokes grid system and the new body force grid system are shown in Figure 5.1.

5.1.2 Interpolation of Original Navier-Stokes solutions

Because of the fact that the grid points were re-distributed for body force extraction, the implementation of an interpolation scheme was also required to interpolate the Navier-Stokes solutions from the original grid system to the new body-force grid system. There are several interpolation schemes available for the implementation, and some of the schemes can be quite sophisticated. Here, one of the simplest methods, i.e. a low-order linear interpolation scheme, was used. This simple scheme basically searches for eight Navier-Stokes grid points that surround each body-force grid point and uses the distances as weighing factors for interpolation.

Having implemented the scheme and interpolated the flow solutions, the post-processed results near the mid span from the interpolated solutions were plotted graphically. The plots are depicted in Figure 5.2. The main purpose of this figure is to compare against that from the original solutions to verify the correct implementation of the scheme. Furthermore, the post-processed flow variables from the interpolation were also mass averaged at each I-index along the axial direction to obtain the profiles that represent one-dimensional total pressure rise and entropy increase. Those two quantities are plotted and presented in Figure 5.3. From the profiles shown in this figure, the solutions were indeed accurately interpolated to produce correct trends of total pressure rise and entropy increase. Since there is no way to compare the interpolated solutions quantitatively against the original solution in this case, it is concluded that the implemented interpolation scheme is consistent based on the qualitative observations.

5.1.3 Extraction of Body Forces

Having verified the correct implementation of the interpolation scheme, the body forces were then modeled and extracted from the interpolated solutions for each computational cell. The use of the low-order linear interpolation scheme lead to an oscillating behavior of flow variables in some regions. This in turn produced oscillations in the magnitudes of the body forces. This could be a consequence of the fact that the interpolation scheme is not quite robust where the cell volumes are considerably small ($\sim 10^{-6}$ m^3). However, mass averaging the body forces with the coarse body force grid system helped suppress the oscillations.

The x-r plots of the body forces resulted from mass averaging are shown in Figure 5.4. Figure 5.4(a) shows pitchwise-averaged axial body force component, and Figure 5.4(b) shows tangentially-averaged pitch-wise body force component. It should be noted that the body forces per unit mass in the figures are normalized by the inlet velocity squared divided by the rotor axial chord.

Figure 5.4(a) indicates that the axial body force near the tip region of the leading edge exhibits the largest magnitude. In addition, the presence of the shock wave near the mid-chord region is clearly reflected due to higher axial body force. The x-r plot of the pitch-wise body force manifests the highest magnitude at the leading edge and a monotonic decay to the trailing edge.

The body forces were mass-averaged at each I-index along the axial direction to examine their one-dimensional behaviors across the blade row region. The resulting profiles are depicted in Figure 5.5. From those profiles in Figure 5.5, the presence of the shock wave can be observed: (1) the axial body force profile has its peak near the location of the shock wave, and (2) the pitch-wise body force decays monotonically until the location of the shock wave, but decays at a higher rate afterwards. The one-dimensional radial body force profile exhibits relatively small magnitudes compared to that of the axial and pitch-wise body forces.

5.1.4 Comments on New Averaging Techniques

It was found that the typical pitch-wise mass- or area-averaging techniques employed to compute the pressure terms in the blade region from the Euler computations are inappropriate. The reason is that the cross sectional area of the Euler grid system at any axial location within the blade row region is greater than that of the original viscous grid system, a result of the blockage caused by the blade is not considered during the Euler computations. Therefore, when averaging, blockage effect should be accounted for in order to compute area-averaged static and mass-averaged total pressures correctly. It can be done as follows:

$$\begin{aligned} P &= C_B \cdot P \\ P_t &= C_B \cdot P + \frac{1}{2}\rho V^2 \end{aligned} \tag{5.1}$$

where $P, P_t, C_B, \rho,$ and V are static pressure, total pressure, a blockage coefficient, density, and velocity vector. The blockage coefficient is the cross sectional area of the original Navier-Stokes grid system divided by that of the Euler grid system. In this case, for example, the blockage coefficient at the mid chord cross section is approximately 0.85. The area- and mass-averaging procedures shown in Equation 5.1 were used in the current work to compute correct static and total pressure from the Euler solutions.

5.1.5 Computational Results

Several Euler computations were carried out initially to slowly raise the magnitudes of the body forces from zero to the final value and to raise the exit static pressure gradually to the specified value. This approach ensures the convergence of the flow variables to the right steady state, as it resembles the physical situation of starting a compressor. The converged solutions were then post-processed to obtain the axial variation of the

pressure, the temperature rise (both total and static), and the velocity components. These are assessed and compared against those from the interpolated Navier-Stokes solutions, and they are shown in Figure 5.6.

The axial velocity and static pressure at each axial location were obtained by using area-averaging technique to conserve mass flow and axial force, respectively. The mass-averaging technique was used for all other variables. The static pressure in the region near the trailing edge of the blade was over-predicted by approximately 5.5 % of the static pressure computed from the Navier-Stokes solutions. Also, it was under-predicted in the upstream region by 5 % of that from the Navier-Stokes solutions. This caused a higher axial velocity in the region also by about 5 % of the axial velocity computed from the Navier-Stokes solutions. However, the two important flow quantities, total-pressure rise and tangential velocity representing the flow turning show excellent agreements. In general, the profiles demonstrate good agreements between the Navier-Stokes and Euler solutions.

Two-dimensional radial profiles at three different axial locations were also generated from both the Euler and Navier-Stokes solutions for comparisons and assessments. As shown in Figure 5.7, the three locations correspond to cross sections at two grid points prior to the leading edge, mid-chord, and two grid points after the trailing edge. The two-dimensional profiles at two grid points prior to the leading edge shown in Figure 5.8 are in good agreement. Matching the upstream conditions ensures that the body forces in the blade region would encounter similar flow conditions as given by the Navier-Stokes solutions. The profiles at the mid chord section in Figure 5.9 indicate that the flow quantities appear to evolve in a manner to yield the same amount of blade work being added into the flow, as should be. Likewise, the comparisons of the profiles at the cross section after the trailing edge shown in Figure 5.10 show a similar trend.

The radial profiles near the end-walls in Figures 5.8, 5.9, and 5.10 show minor inconsistencies between the Euler and Navier-Stokes solutions. There are two main reasons for these. The first is that the shear forces near the end-walls in the upstream

region were not modeled, causing a mismatch of the profiles near the end-walls prior to the leading edge. Since the flow conditions near the end-walls at this section are not identical, all subsequent downstream profiles near the end-walls would not be matched. A solution to this problem is suggested in Chapter 6. The second could be due to the fact that an Euler solver using different wall boundary conditions was employed to obtain the solutions. The differences had altered the profiles near and on the wall boundaries. The comparison of the pressure rise characteristics at the given operating point in Figure 5.11 also shows excellent agreement.

If a higher accuracy is desired, additional refinements can be implemented. These include improving the interpolation scheme and accounting for the effects of upstream end-wall boundary layers using body forces. Even without these refinements, the present results show that the use of an Euler solver with an embedded body force representation of a blade row yields a flow and blade-row performance in accord with that given by the Navier-Stokes solutions.

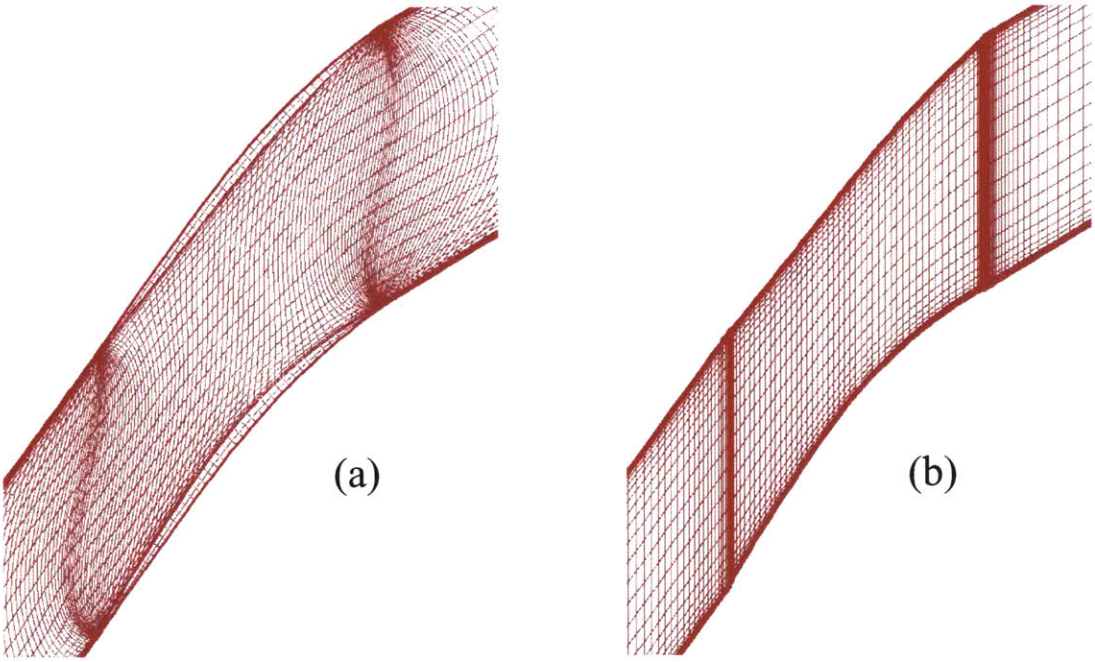

Figure 5.1: (a) Original Navier-Stokes grid system and (b) body-force grid system

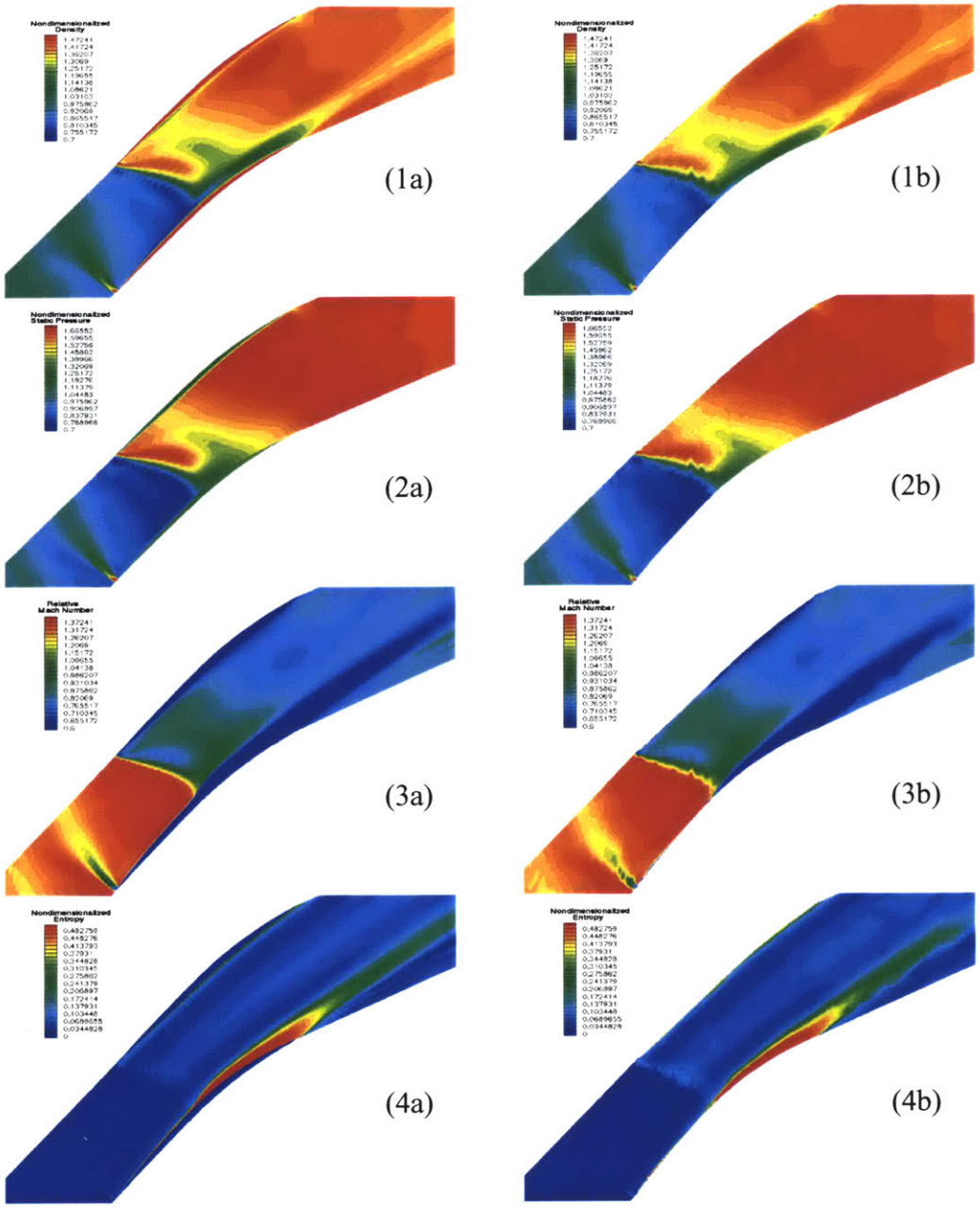

Figure 5.2: Comparisons of flow quantities between the original Navier-Stokes solutions and the interpolated solutions: (a) and (b) represent plots from the original and the interpolated solutions, respectively. The flow quantities shown here are (1) density, (2) static pressure, (3) relative Mach number, and (4) entropy. All quantities are normalized.

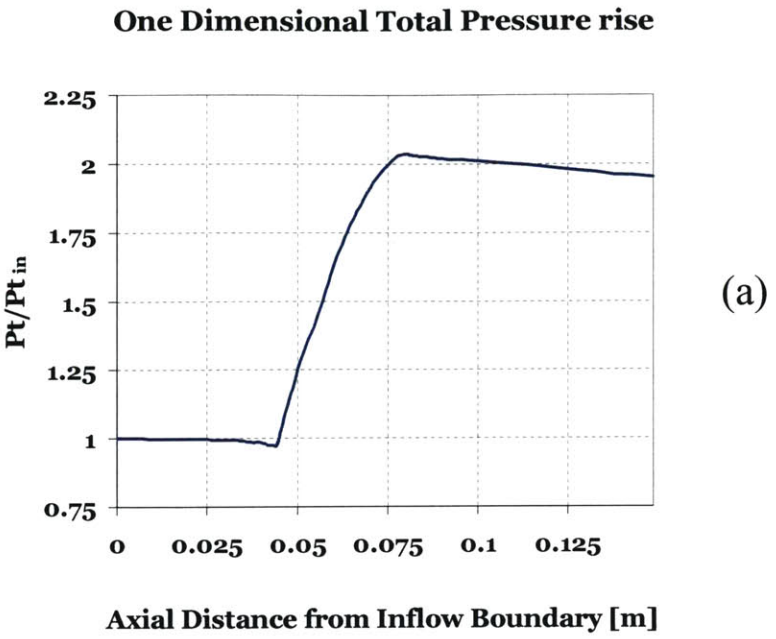

(a)

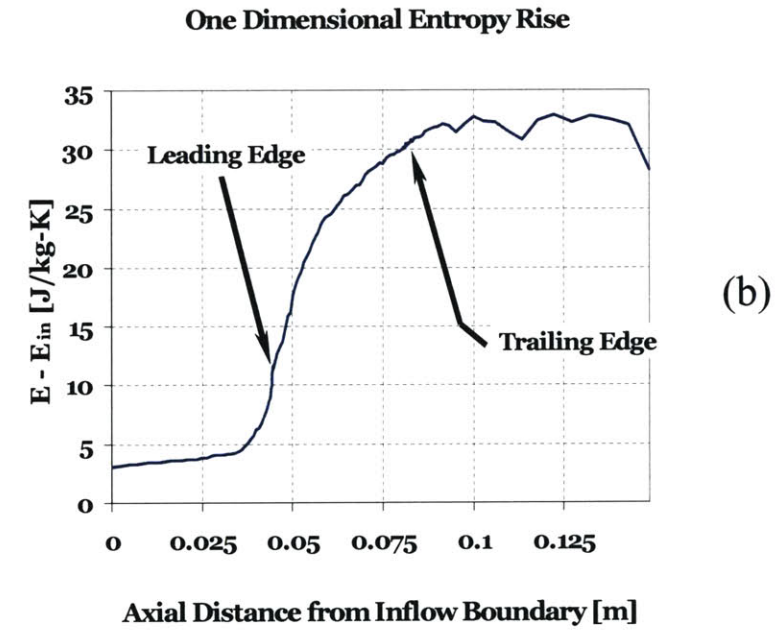

(b)

Figure 5.3: Mass-averaged one-dimensional profiles of (a) total-pressure rise and (2) entropy rise in the axial direction obtained from the interpolated solutions

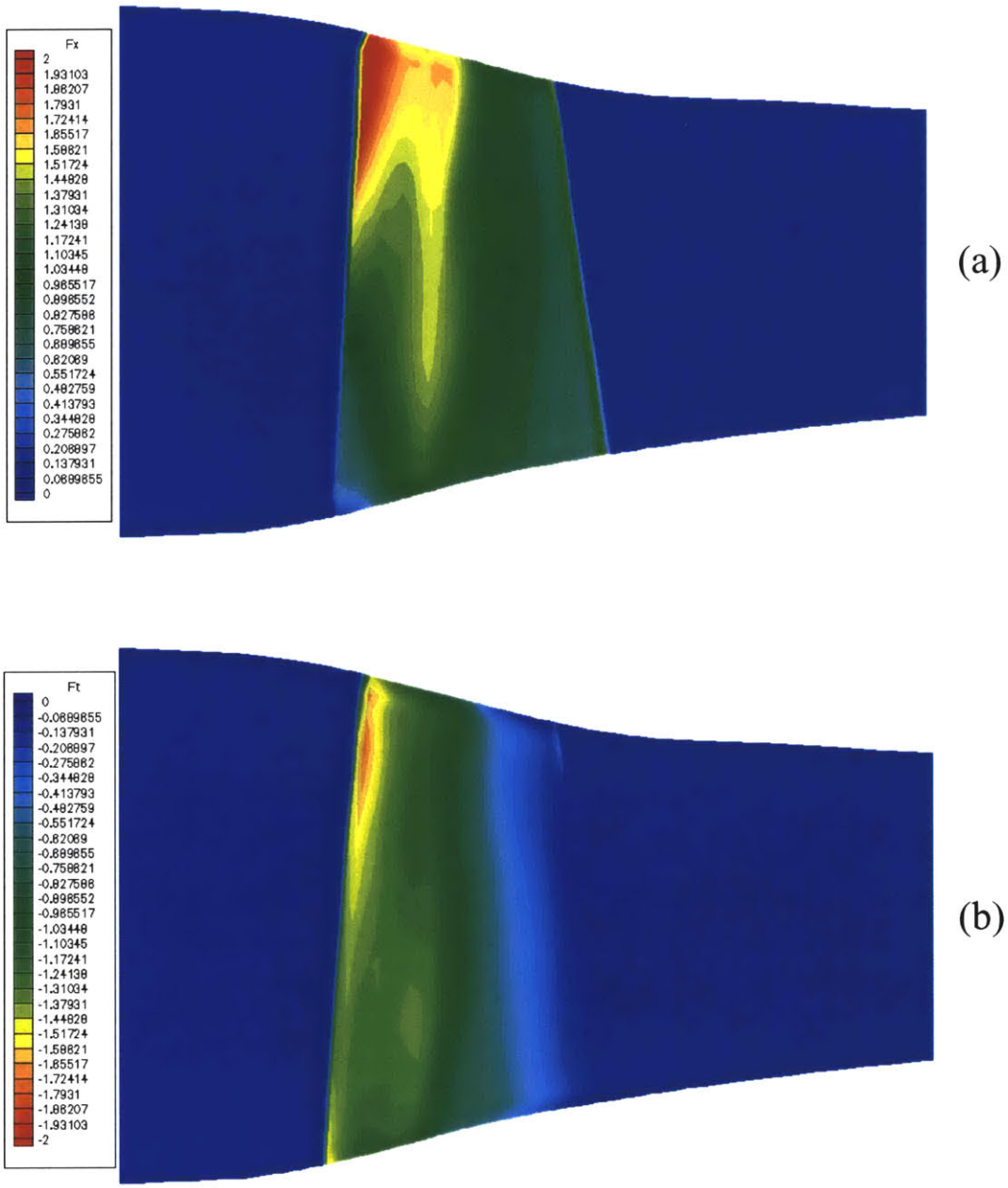

Figure 5.4: Pitch-wise-averaged body forces: (a) axial body force and (b) tangential body force

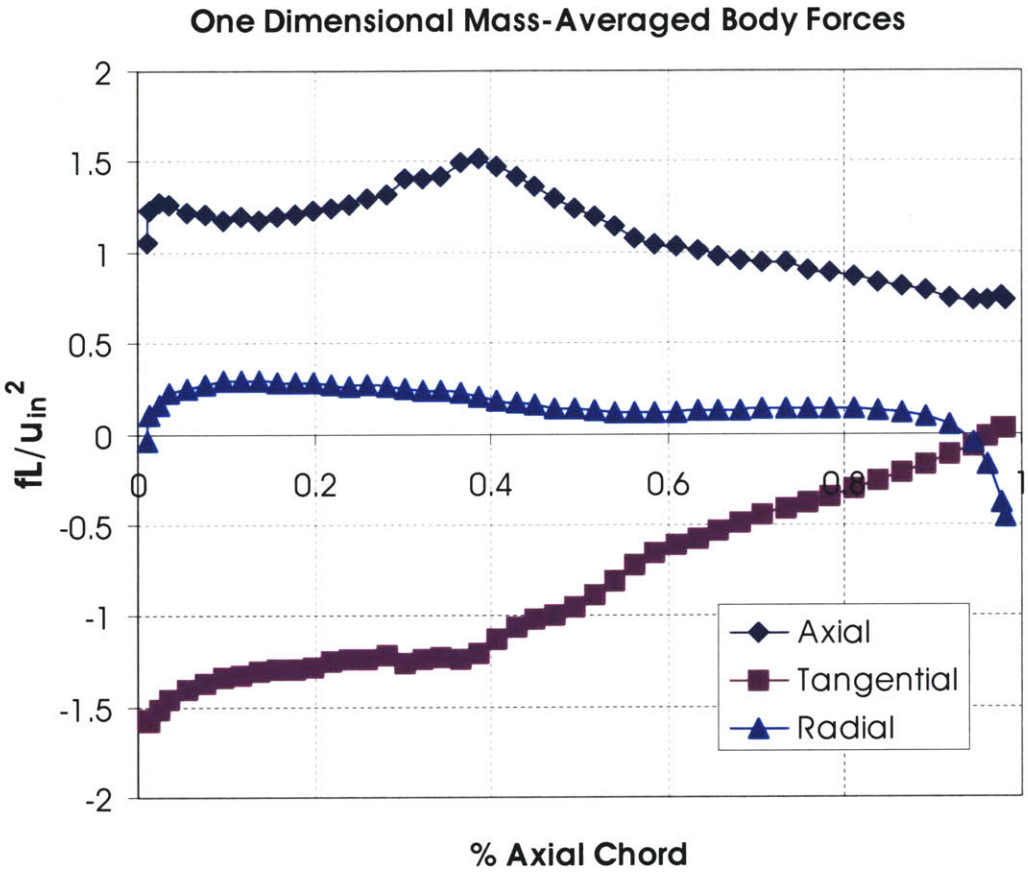

Figure 5.5: One-dimensional profiles of mass-averaged body-forces

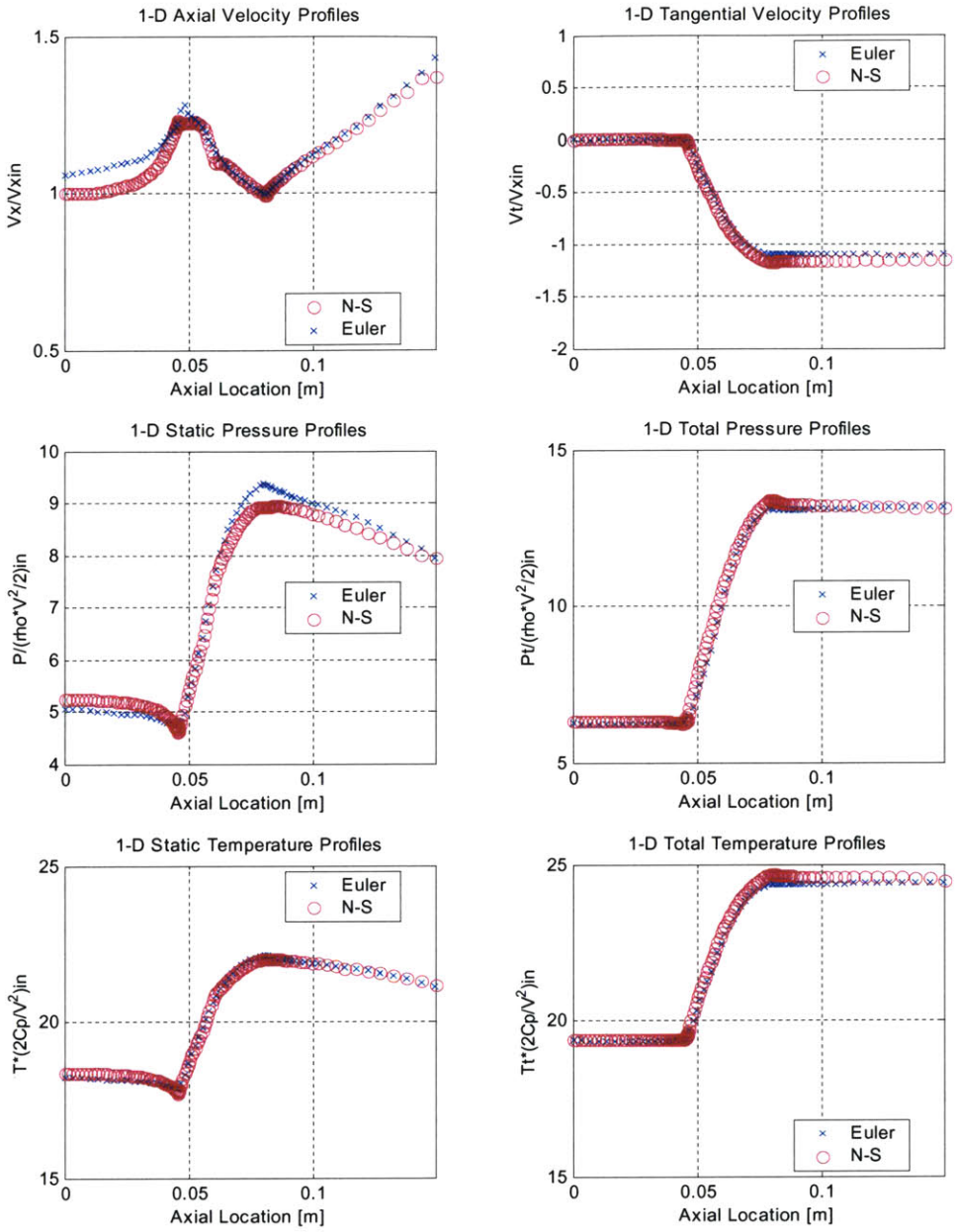

Figure 5.6: Comparisons of one-dimensional profiles of averaged flow solutions. All quantities are mass averaged except axial velocity and static pressure for which area-averaging technique was used.

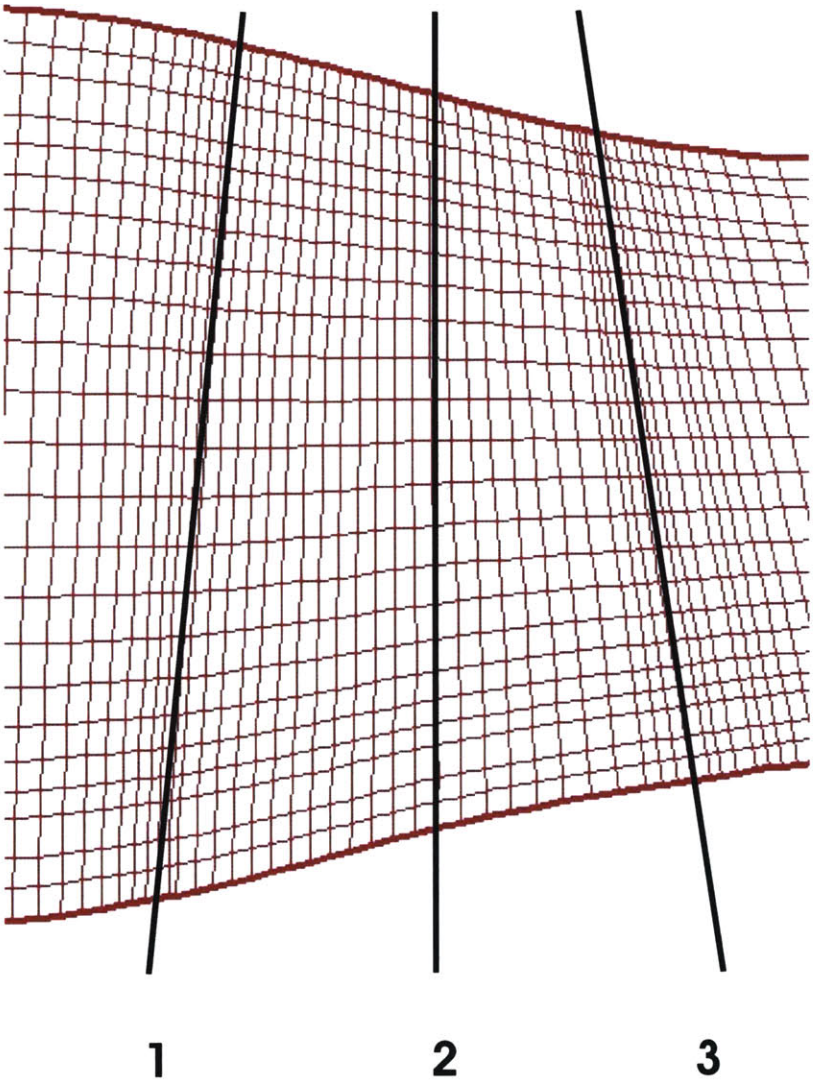

Figure 5.7: Illustration of cross sections chosen for comparisons of two-dimensional radial profiles: (1) two grid points prior to the leading edge, (2) mid-chord, and (3) two grid points after the trailing edge

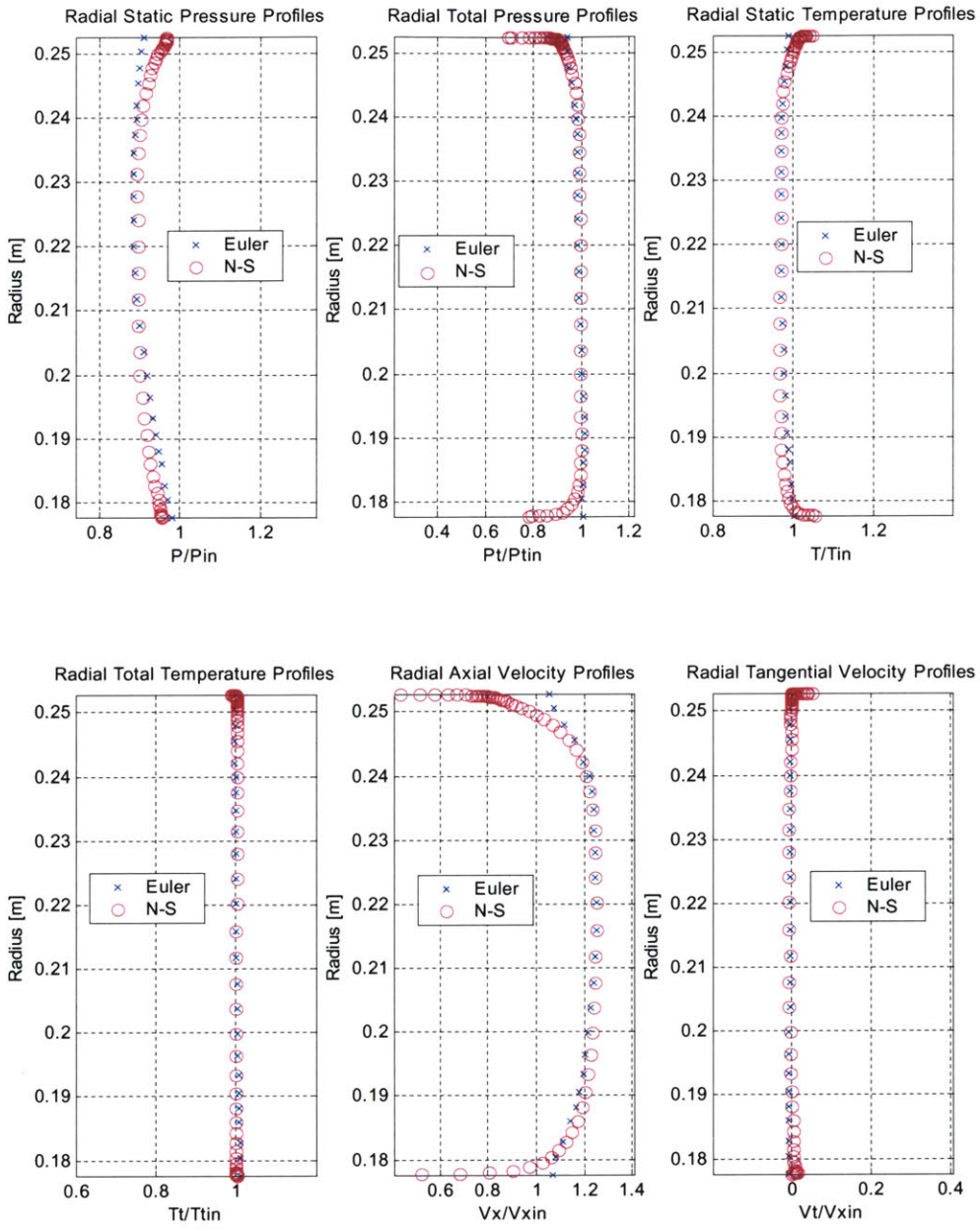

Figure 5.8: Comparisons of radial profiles prior to the leading edge from the first test case

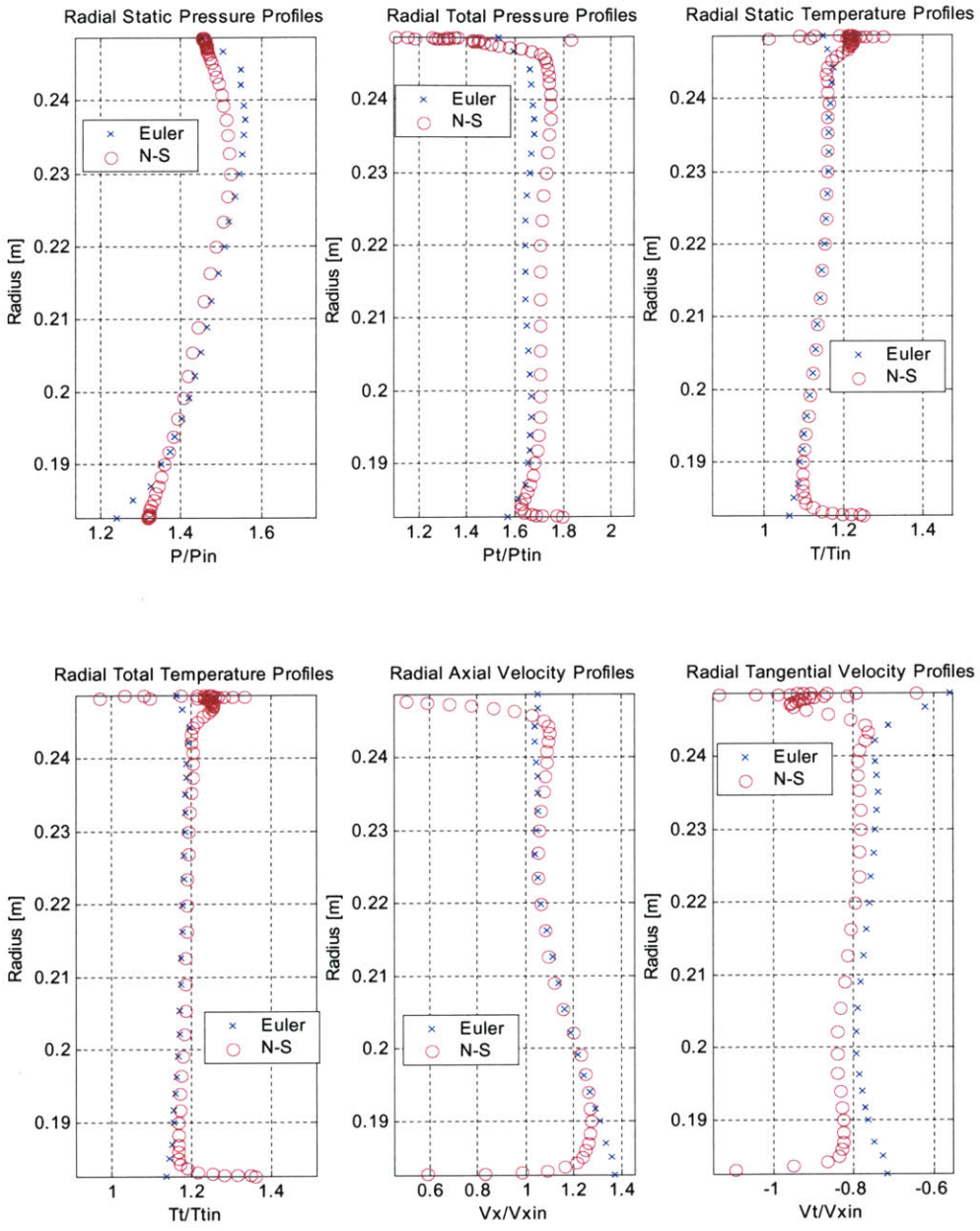

Figure 5.9: Comparisons of radial profiles at the mid-chord from the first test case

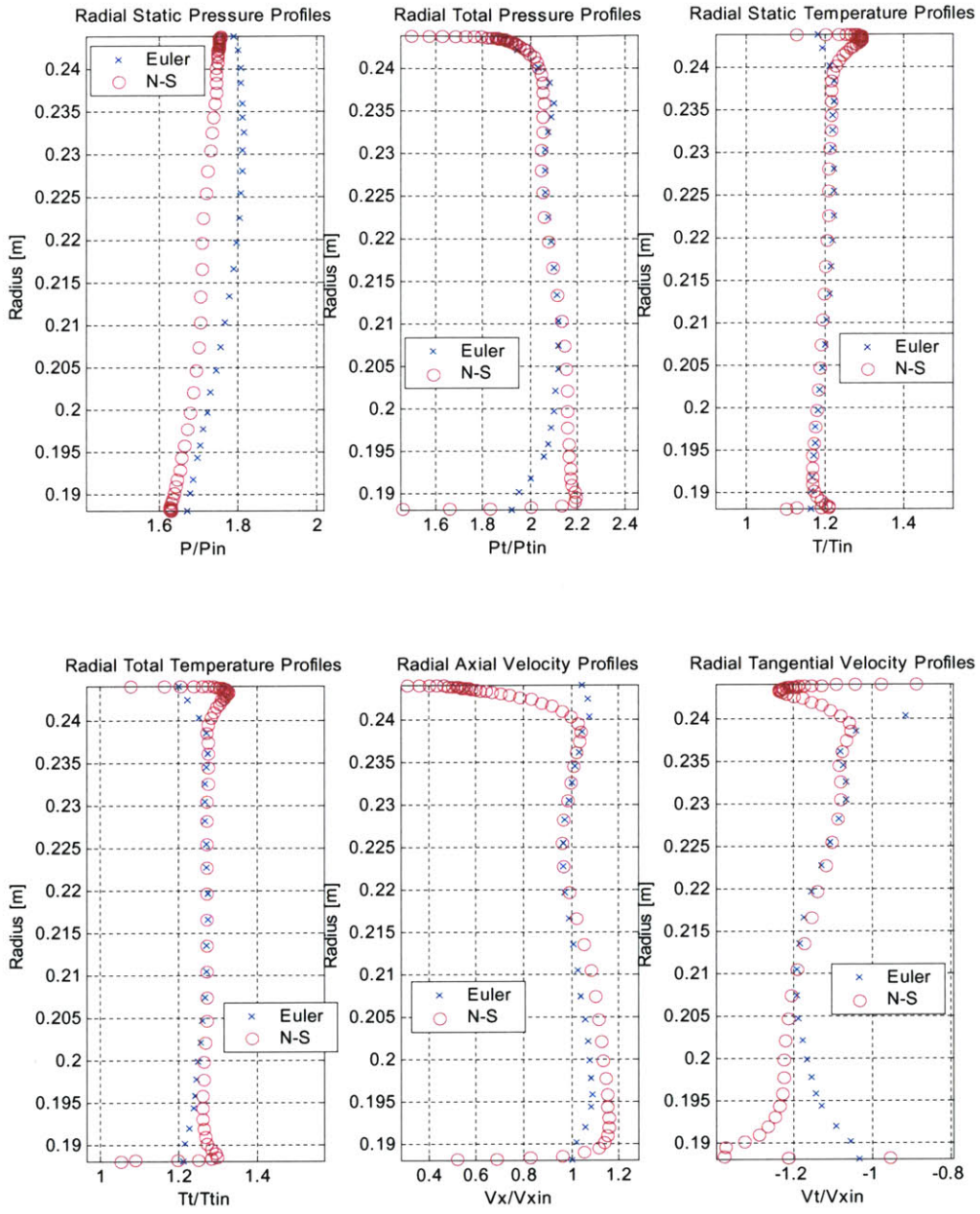

Figure 5.10: Comparisons of radial profiles after the trailing edge from the first test case

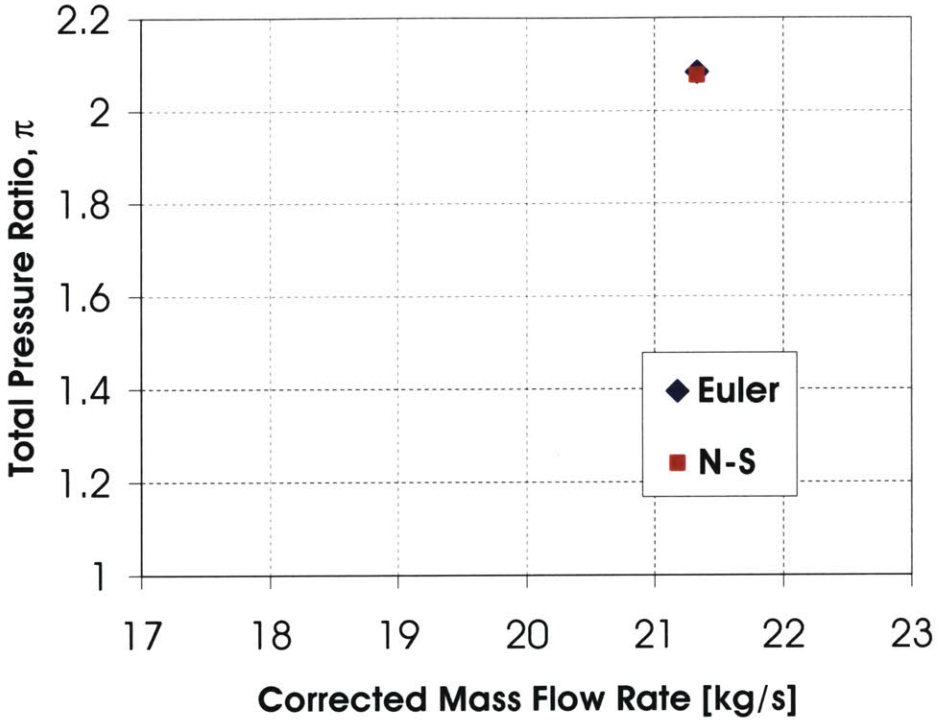

Figure 5.11: Comparisons of pressure-rise characteristics from the first test case

5.2 Test Case 2: Redistribution of Body forces

For the second test case, a body force database was generated by adapting the procedures introduced in Sections 5.1.1, 5.1.2, and 5.1.3. The local relative Mach numbers in the blade row region were used as the controlling parameter to determine the magnitudes of the body forces. The resulting database contains three relative Mach numbers and their corresponding body force components for each computational cell in the body force grid system. As mentioned previously, a linear interpolation was used to approximate the magnitudes between any two relative Mach numbers. Also, the averaging techniques derived in Section 5.1.4 were used to post-process both the static and the total pressure after the Euler computations have been completed.

Using the body force database generated, the replication of operating point 4, shown in Figure 4.5, was first selected for further validating the applicability of the approach. Inflow and outflow boundary conditions constructed from the Navier-Stokes solutions at this operating point were used to compute the flow field. As in the first test case, a number of computations was carried out to "pre-condition" the flow field by gradually raising the body forces and exit static pressure from zero to the final/specified value at a 10-percent interval of the final value. To approximate the exit static pressure, which is required for the first initial computation with vanishing body force distribution in the blade row, the Bernoulli equation was used assuming constant inlet density through the flow domain. The body forces and the exit static pressure were raised until the mass flow was matched. One- and two-dimensional profiles obtained from the converged solutions are presented in Figures 5.12, 5.13, 5.14, and 5.15.

The averaged one-dimensional profiles in Figure 5.12 show good agreements. All the flow quantities obtained from the Euler solutions except the axial velocity profile exhibit no major deviations from that of the original Navier-Stokes solutions. Nevertheless, the

axial velocity profiles for this test case are considerably well matched compared to the first test case.

From the comparisons of the two-dimensional profiles, it is deduced that the relative Mach number is indeed adequate to redistribute the body forces in the supersonic flow regime. This deduction is based on the excellent agreements shown in Figures 5.13, 5.14, and 5.15. However, mismatches in the tangential velocity profiles at the mid chord and after the trailing edge indicate that the amount of work added to the flow near the end-wall boundaries may not be quite accurate. This problem was also observed in the first test case. The suggested solution provided in Chapter 6 can resolve this discrepancy observed in the end walls.

Two additional Euler computations were carried out to simulate the pressure-rise characteristics of the rotor at operating points 3 and 5 starting from the converged solutions at point 4. These operating points are denoted in Figure 4.5. Detailed one- and two-dimensional profiles obtained from the converged solutions at the two additional operating points are not shown here as there are no noticeable differences.

Instead, pressure-rise characteristics computed from the Euler solutions are compared against that from the Navier-Stokes solutions for all three operating points; these are presented in Figure 5.16. The figure shows that the pressure-rise characteristics were well predicted with a maximum discrepancy of approximately 2.3 % of the peak pressure rise. From this comparison, it can be concluded that the computational methodology developed in the current work is capable of redistributing the body forces on a consistent basis.

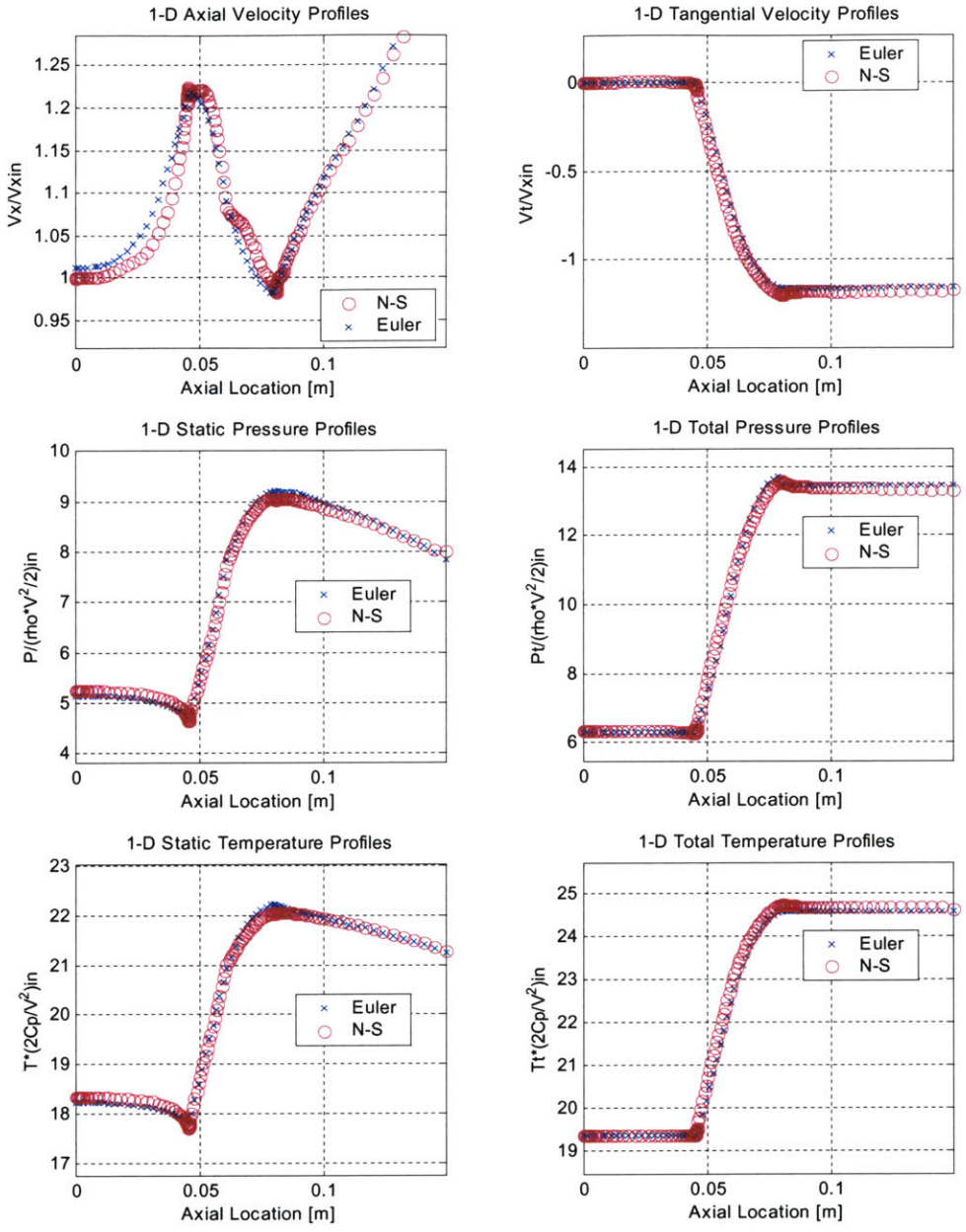

Figure 5.12: Comparisons of one-dimensional profiles of averaged flow solutions from the operating point number 4. All quantities are mass averaged except axial velocity and static pressure for which area-averaging technique was used.

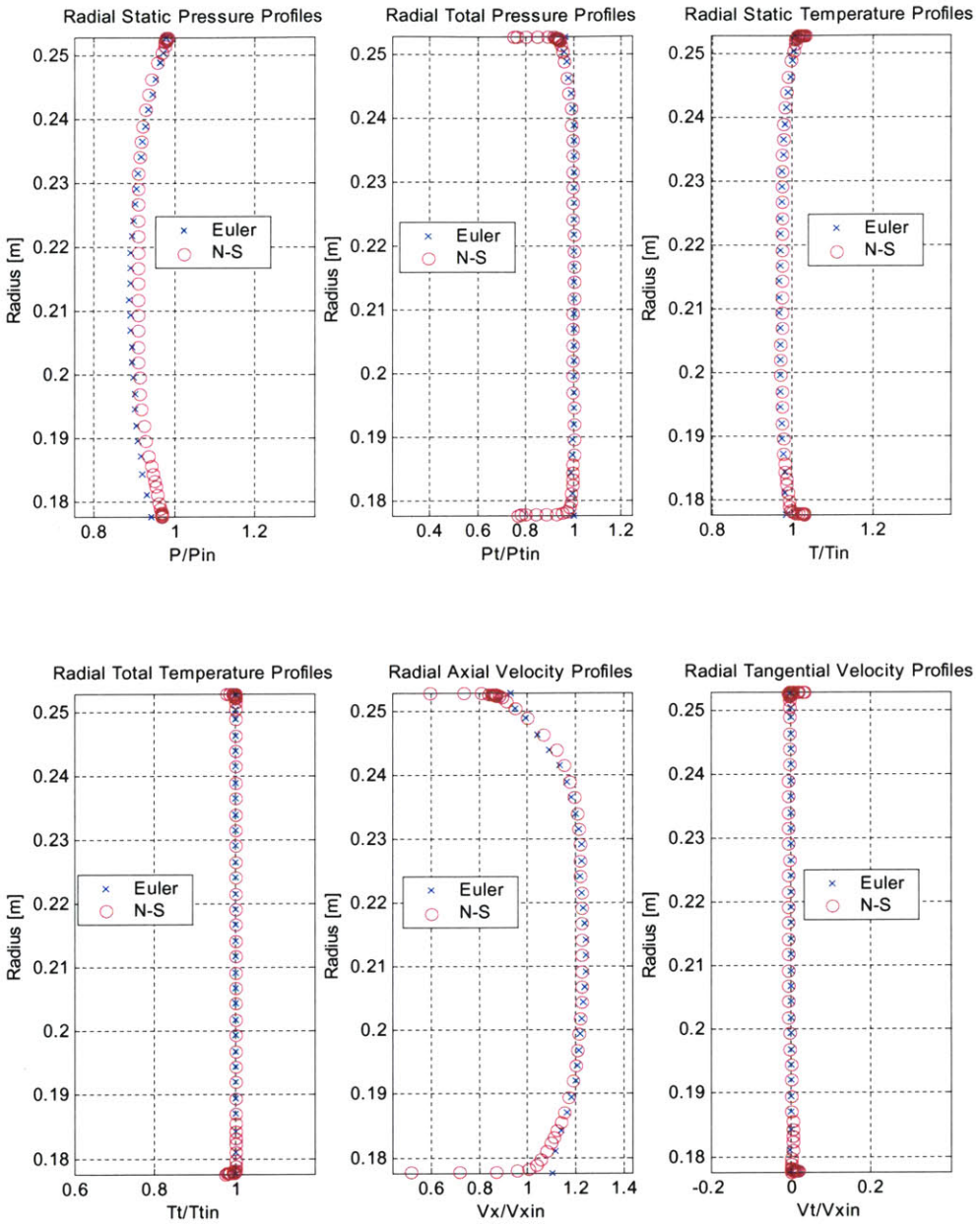

Figure 5.13: Comparisons of radial profiles prior to the leading edge from operating point 4

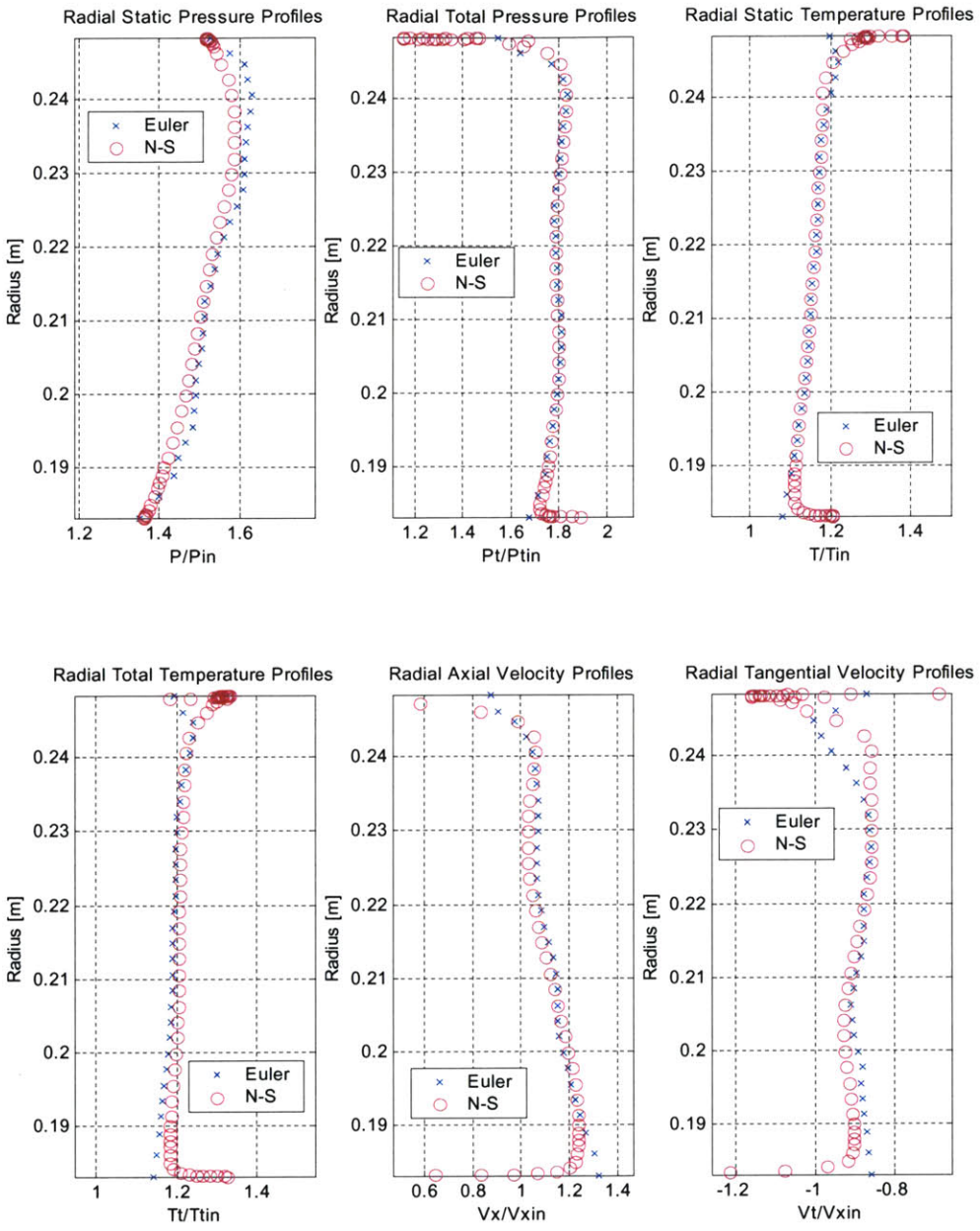

Figure 5.14: Comparisons of radial profiles at the mid-chord from operating point 4

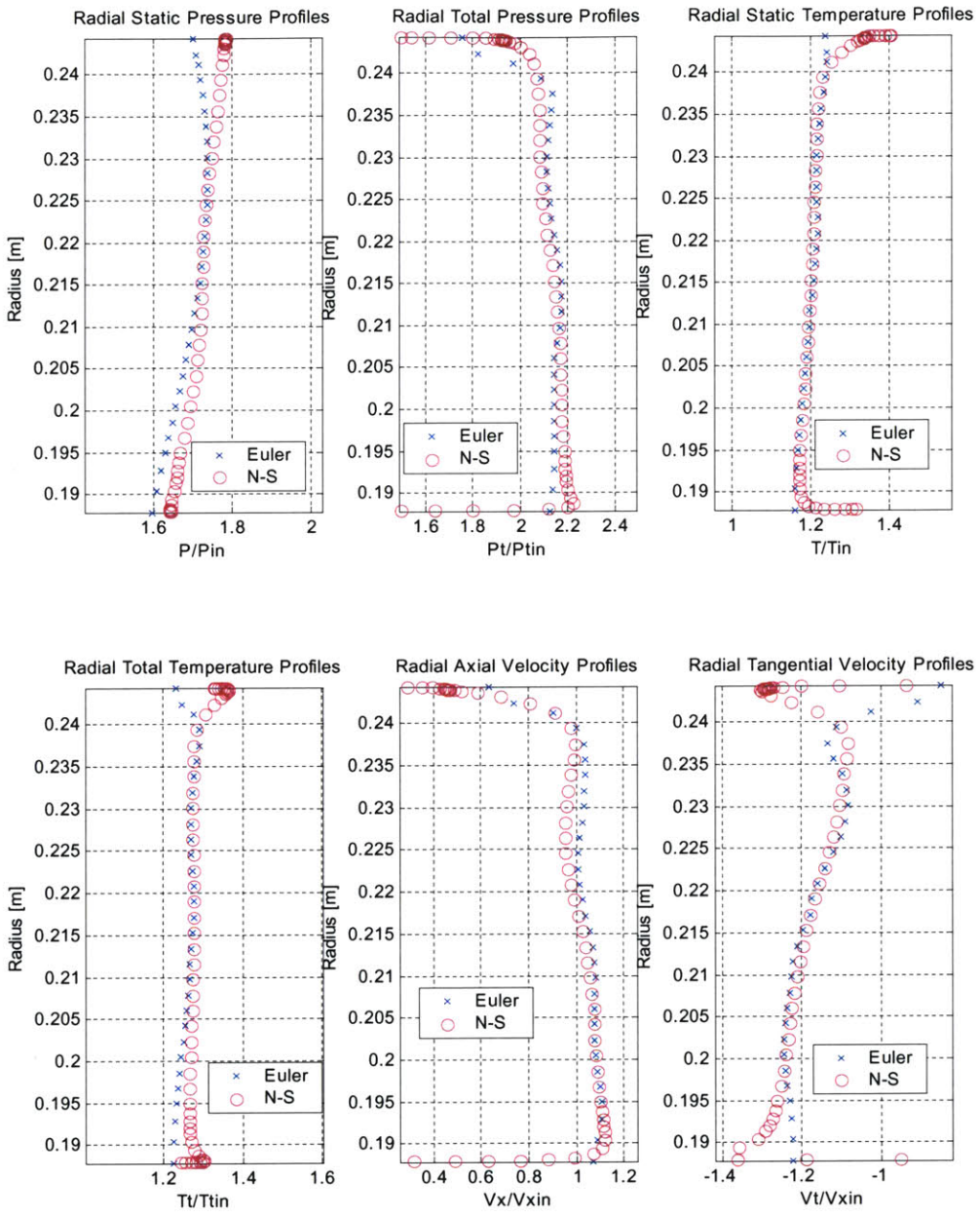

Figure 5.15: Comparisons of radial profiles after the trailing edge from operating point 4

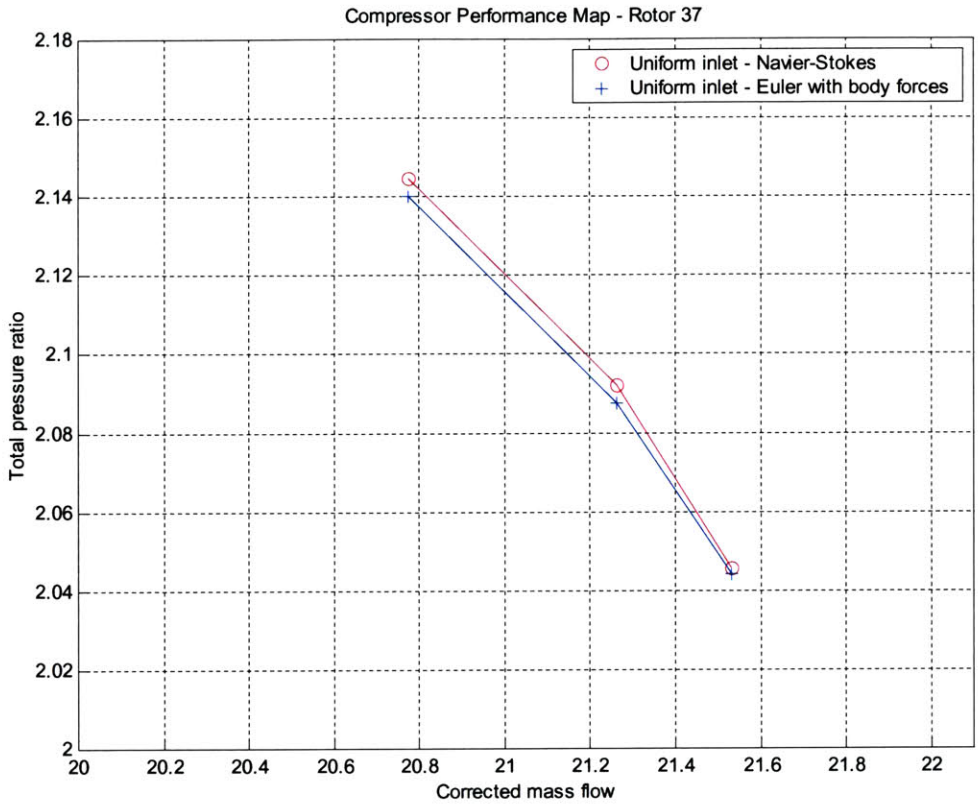

Figure 5.16: Comparisons of pressure-rise characteristics for three operating points from which the body-force database was generated

5.3 Test Case 3: Radial Inlet Distortions

The steady state Euler solutions were obtained by applying the inflow and outflow boundary conditions constructed from the Navier-Stokes solutions with the radial inlet distortions. The converged solutions from operating point 4, shown in Figure 4.5, were selected as the initial conditions for this computation. The steady state solutions for this test case were achieved after 30,000 iterations. No manual "pre-conditioning" was necessary since the overall operating conditions between operating point 4 and the radial distortion case were similar. As in previous cases, the exit static pressure was adjusted to match the mass flow rate.

One-dimensional profiles that delineate the axial variations of the flow variables across the blade row are shown in Figure 5.17. It can be seen that the tangential velocity after the trailing edge was under-predicted by approximately 5 % of that from the Navier-Stokes solutions. This also caused the total-pressure rise and the total-temperature rise to be approximately 1.0 % and 1.2 % less when compared to the total-pressure rise and the total-temperature rise computed from the Navier-Stokes solutions, respectively. Although the actual magnitudes of the static pressure and temperature near the inflow and outflow boundaries were differed from the Navier-Stokes solutions by a maximum of approximately 6 % of the static pressure at the exit, the pressure and temperature rises across the blade row were well predicted. In general, two-dimensional profiles also show good agreements, except near the end-wall boundaries, as in previous test cases.

The comparison of the pressure-rise characteristics subjected to the radial inlet distortions presented in Figure 5.16 indicates that the Euler computation with the body force formulation well captured the overall change of the rotor performance. The pressure-rise predicted by the body force formulation was found to be also less than that from the corresponding Navier-Stokes solutions by 1.2 % of the pressure-rise, exhibiting the same trend as in the uniform inlet cases.

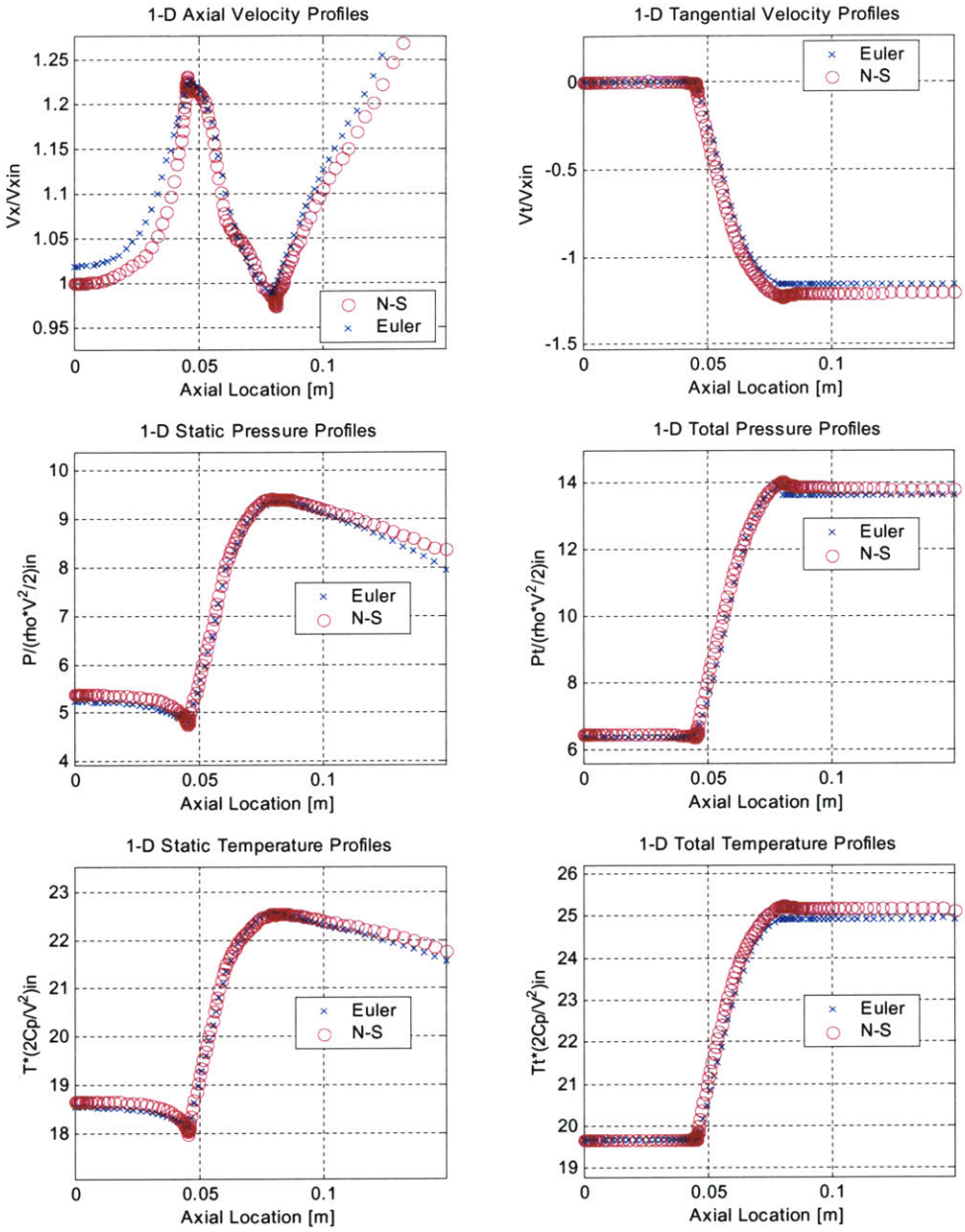

Figure 5.17: Comparisons of one-dimensional profiles of averaged flow solutions from the radial inlet distortion case. All quantities are mass averaged except axial velocity and static pressure for which area-averaging technique was used.

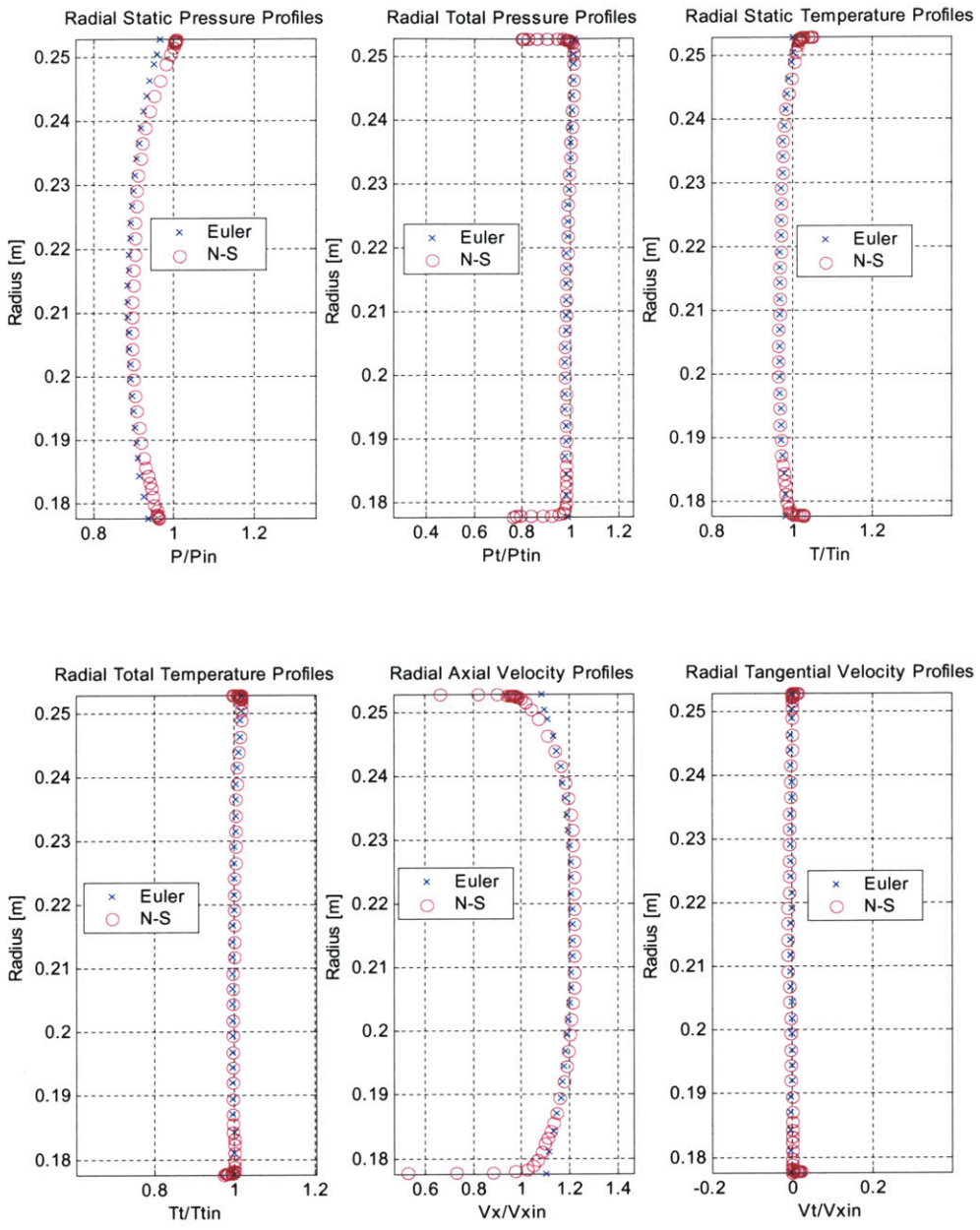

Figure 5.18: Comparisons of radial profiles prior to the leading edge from the radial inlet distortion case

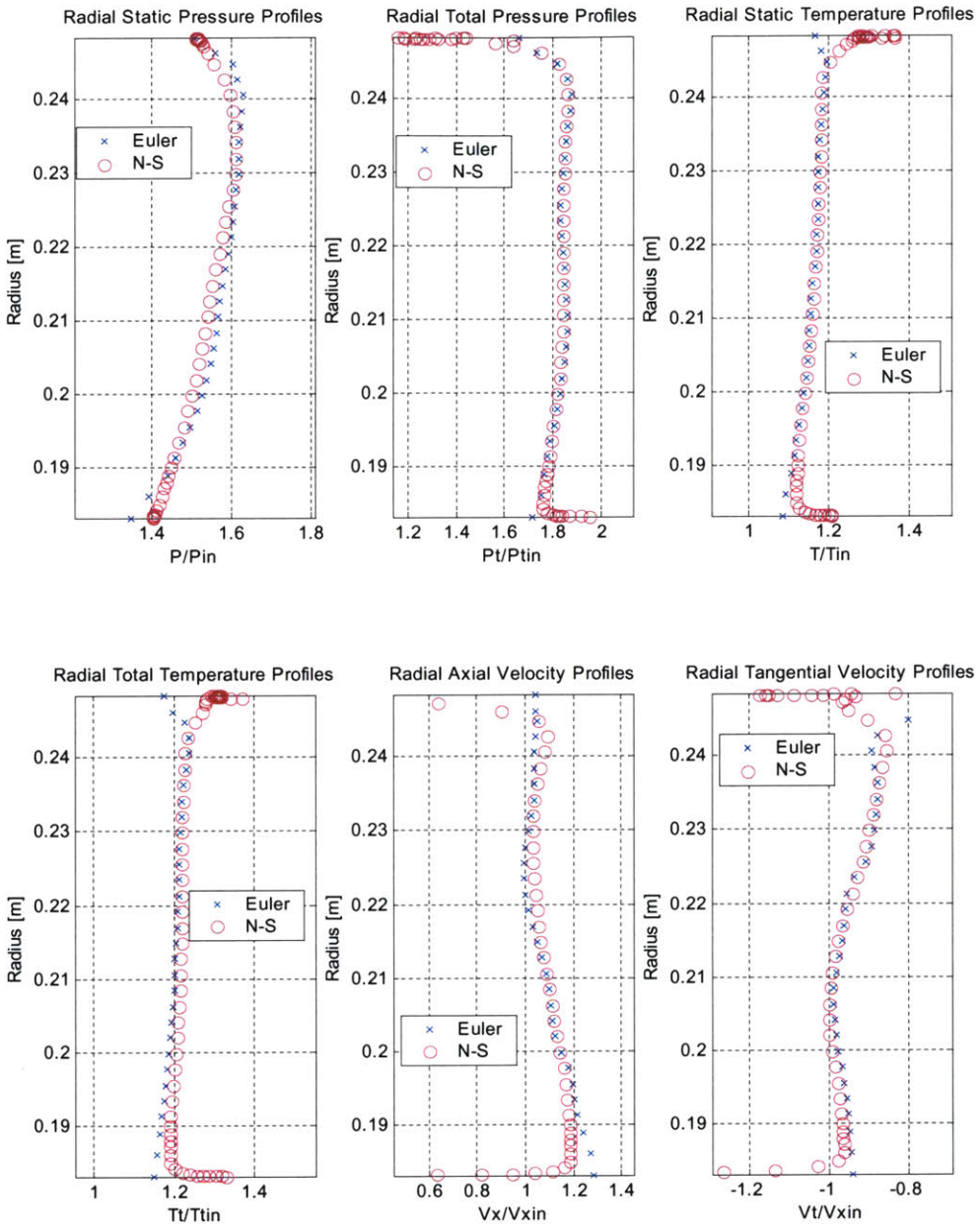

Figure 5.19: Comparisons of radial profiles at the mid-chord from the radial inlet distortion case

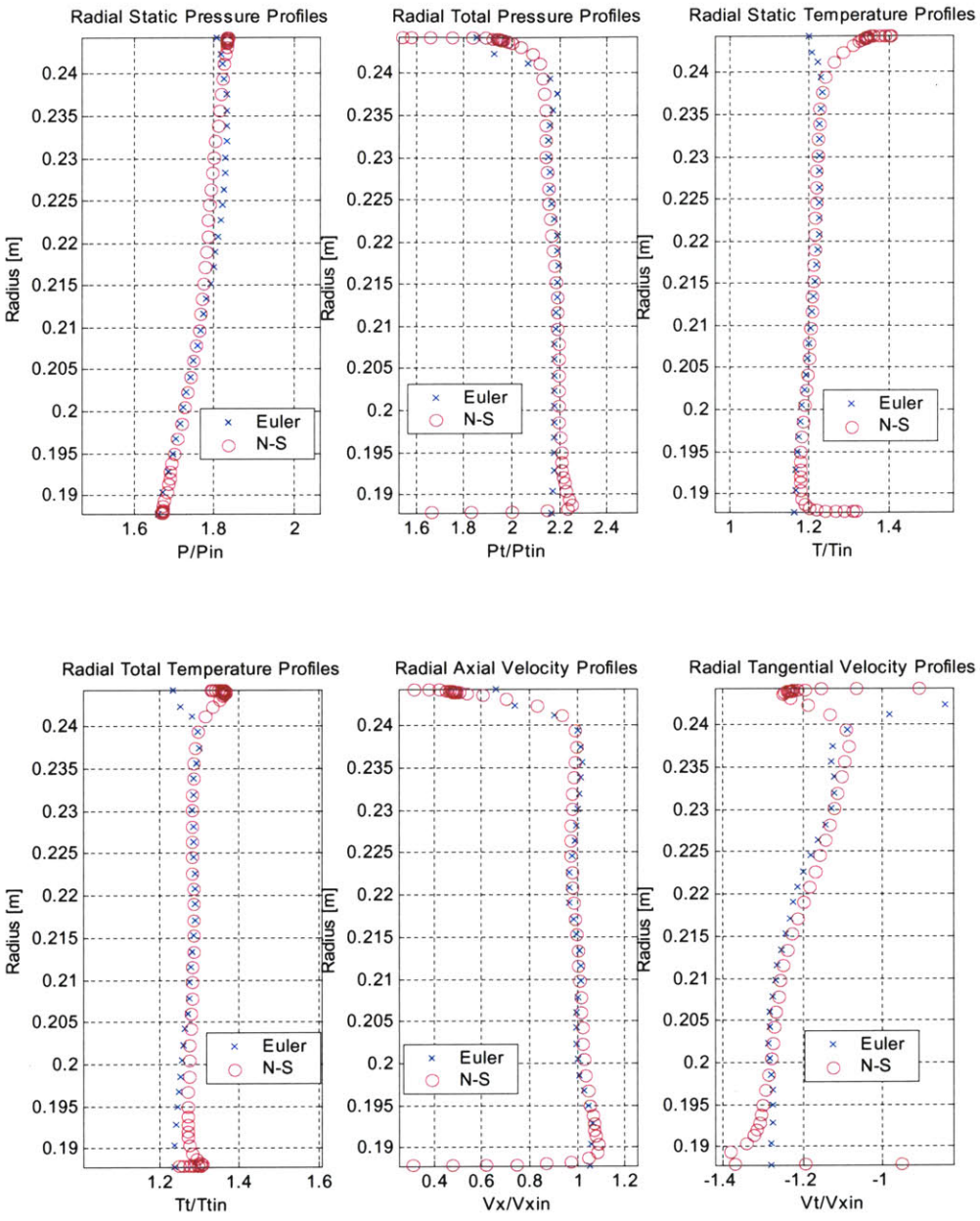

Figure 5.20: Comparisons of radial profiles after the trailing edge from the radial inlet distortion case

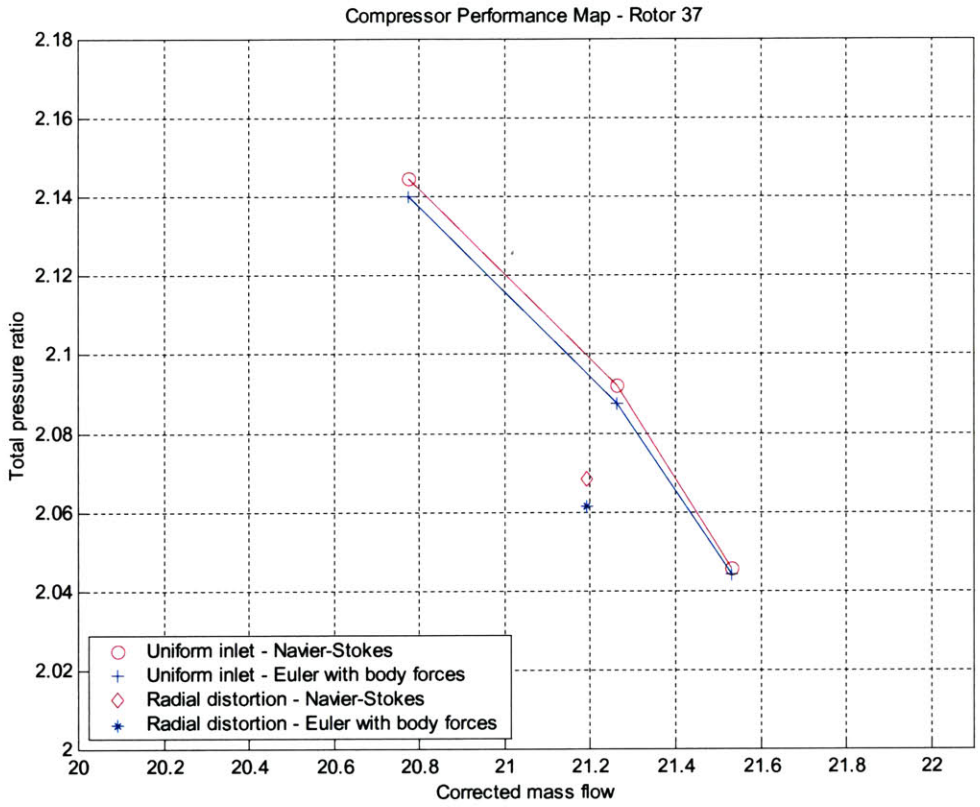

Figure 5.21: Comparisons of pressure-rise characteristics between the uniform inlet and radial inlet distortion cases

5.4 Test Case 4: IGV-Rotor-Stator Configuration

At the time of this thesis being completed, the multi-stage simulation using the body force database was still in progress. Therefore, this section is devoted to describing how the simulation was being carried out rather than presenting the final results.

As in the first two test cases, the flow was also being "pre-conditioned" by gradually raising the body forces. First, the Bernoulli equation was used to approximate analytically the exit static pressure required to start the computation. The constant density assumption was also made to do this. Second, starting from the upstream IGV blade row, the magnitudes of the body forces were slowly raised from zero to final value at 20-percent interval of the final value. Once the body forces in the IGV blade row region were raised up to the final value, the body forces representing the middle rotor blade row were then started to be raised from zero to the final value and so on, until the body forces in all three blade rows were all raised up to the final value. The exit static pressure was controlled manually at each pre-conditioning step to allow the flow field to reach a steady state.

Figure 5.17 shows preliminary one-dimensional results obtained from the multi-stage computation. In this figure, the overall mass flow was not completely matched by approximately 5.6 % of the mass flow computed from the Navier-Stokes solutions. Therefore, strictly speaking, the profiles in the figure do not provide any significant physical meanings and conclusions regarding the applicability of the formulation for a multi-stage compressor. However, the preliminary comparisons are encouraging in that the computational methodology developed here can potentially be used for predicting the performances of multi-stage compressors. This is so as the overall trends across the three blade rows are well captured. The completion of the computation and final comparisons are left as the first part of future work.

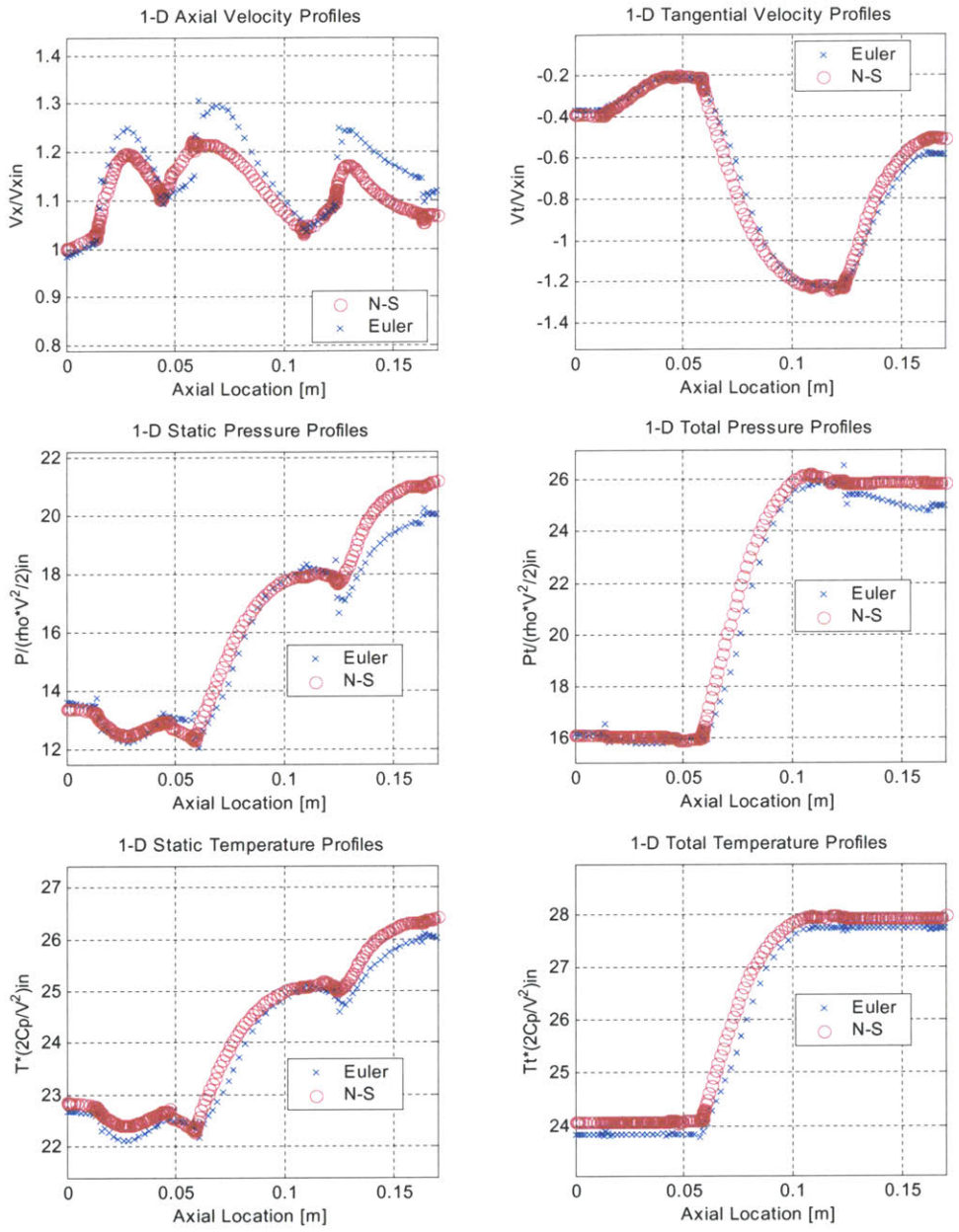

Figure 5.22: Preliminary results showing one-dimensional profiles of averaged flow solutions from the multi-stage configuration. All quantities are mass averaged except axial velocity and static pressure for which area-averaging technique was used.

CHAPTER 6

SUMMARY, CONCLUSIONS, AND FUTURE WORK

6.1 Summary and Conclusions

The objective of this thesis was to develop an adequate and effective computational methodology for efficient multi-stage compressor map generation. While the computation on a multi-blade-row configuration (IGV-rotor-stator) has not been carried out to completion to generate a performance map, the validity and soundness of the approach was demonstrated during the course of the research project based on the single-blade row calculations. The purpose of this section is to summarize the work and present the conclusions.

6.1.1 Summary

The development of the computational methodology consists of using a few isolated-blade row Navier-Stokes solutions for each blade row to construct a body force database. The purpose of the body force database is to replace each blade row in a multi-stage compressor by a body force distribution to produce same pressure rise and flow turning. To do this, each body force database is generated in such a way that it can respond to the changes in local flow conditions and redistributes itself instantaneously. Once the database is generated, no further Navier-Stokes computations are necessary. The process

is repeated for every blade row in the multi-stage compressor. Numerical predictions under a new set of inflow and outflow boundary and operating conditions can be carried out by using an Euler code with the body force databases.

In Chapter 2, the overall computational procedures for the concept validation as well as for the flow analysis with a body force database were developed. Also, a few advantages of the new computational methodology over the conventional CFD approaches were described: they include modeling simplicity and significant reductions in computational costs. The body forces were first computed in Cartesian coordinates by solving the integral form of the momentum equations, and subsequently transformed to that in cylindrical coordinates by using a rotation matrix. The corresponding body forces were embedded as source terms in the Euler equations; they were solved iteratively by using a standard finite volume method with an explicit four-stage Runge-Kutta scheme.

A dimensional analysis was carried out in Chapter 3 to determine the local flow conditions that parameterize the magnitudes of the body forces. Useful engineering applications using the current computational methodology were suggested: (1) a performance prediction of a single rotor blade row subjected to radial inlet distortions and (2) a prediction of performance and flow distribution in a multi-stage compressor.

Four test cases were performed to assess the physical consistency of the methodology. The first three test cases made use of the NASA Rotor 37, a single rotor blade row. The last test case consisted of an IGV-rotor-stator configuration of a high-pressure compressor with a high bypass ratio. For each test case, detailed descriptions of the investigated blade row, grid dimensions of both Navier-Stokes and Euler computations performed, and operating conditions under which the test case was carried out were delineated in Chapter 4. All the corresponding computational results from the test cases and their comparisons against the Navier-Stokes solutions are given in Chapter 5. Conclusions deduced from the computational results are provided in the next sub-section.

6.1.2 Conclusions

In general, the body forces can be parameterized in terms of the two relative flow angles, the relative Mach number and the Reynolds number when the flow relative to the blade is subsonic. For high-speed transonic flows, they can be parameterized in terms of local relative Mach number alone.

The physical consistency of the methodology developed in the present thesis was validated by the excellent agreements of both the one-dimensional variations and two-dimensional profiles of the flow quantities as well as the compressor performance obtained from the first test case. The performance of a compressor blade row at a new operating point can be accurately predicted by using the body force database, which is created from the Navier-Stokes solutions with uniform inlet conditions. This capability was shown in the second test case. The third test case showed that the flow field subjected to radial inlet distortions could be predicted using the same body force database. The conclusions deduced from the first three test cases together with the preliminary results on the IGV-rotor-stator configuration computation demonstrated the utility of the methodology for predicting the performance and the flow distribution in a multi-stage compressor.

6.2 Recommendations for Future Work

The work in this thesis demonstrated the capability of the methodology to compute the blade row performance subjected to radial inlet distortions based on the body forces constructed from a few Navier-Stokes solutions with uniform inlet conditions. The applicability of the methodology for predicting compressor performance subjected to circumferential inlet distortions has to be shown as well. The body force database developed for the NASA Rotor 37 in the second and third test case can be used to assess this applicability readily. It is anticipated that the current body force model will

successfully simulate the flow under these non-uniform conditions, since the body force database was able to respond to the changes in local conditions.

The preliminary results from the multi-stage computations show that the methodology is promising for a multi-stage compressor. Therefore, the completion of the multi-stage computations and assessment of the applicability of the methodology by comparing the results against the multi-stage Navier-Stokes solutions are suggested as the second phase of the future work.

While the results presented in this thesis are for a high-speed transonic blade row where the body forces can be parameterized in terms of the local relative Mach number, it is suggested that a subsonic blade row should be considered. Here, the body forces will have to be parameterized in terms of the local relative Mach number, and the two local relative flow angles as well.

The radial profiles near the end-walls of a blade row can be improved by modeling the body forces created by the viscous effects, as shown in Figure 6.1, in the upstream region of the blade row. The implementation is relative simple and should be incorporated into the Euler code.

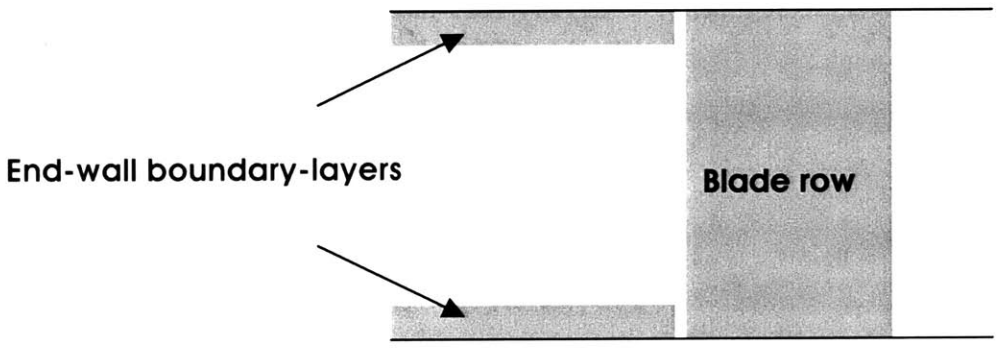

Figure 6.1: End-wall boundary layer model

Finally, stability characterization of a multi-stage compressor using the current methodology would be a powerful application. The stability characterization includes predictions of stall inception associated with both long- and short-wave disturbances.

REFERENCES

[1] Adamczyk, J. J., "Model Equation for Simulating Flows in Multistage Turbomachinery," ASME Paper No. 85-GT-226, 1985.

[2] Billet, G., Huard, J., Chevalier, P., and Laval, P., "Experimental and Numerical Study of the Response of an Axial Compressor to Distorted Inlet Flow," ASME JOURNAL OF FLUIDS ENGINEERING, Vol. 110, 1988, pp. 355-360.

[3] Cumpsty, N. A., Compressor Aerodynamics, Longman, 1989.

[4] Denton, J. D., "The Use of a Distributed Body Force to Simulate Viscous Effects in 3D Flow Calculations," ASME Paper 86-GT-144, 1986.

[5] Dring, R. P., and Spear, D. A., "The Effects of Wake Mixing on Compressor Aerodynamics," ASME JOURNAL OF TURBOMACHINERY, Vol. 113, 1991, pp. 600-607.

[6] Escuret, J. F., and Garnier, V., "Numerical Simulations of Surge and Rotating Stall in Multi-Stage Axial-Flow Compressors," AIAA Paper 94-3202, 1994.

[7] Fay, J. A., Introduction to Fluid Mechanics, MIT Press, 1994.

[8] Gong, Y., Tan, C. S., Gordon, K. A., Greitzer, E. M., "A Computational Model for Short-wavelength Stall Inception and Development in Multistage Compressors," ASME JOURNAL OF TURBOMACHINERY, Vol. 121, 1999, pp. 726-734.

[9] Hetherington, R., and Moritz, R., "The Influence of Unsteady Flow Phenomena on the Design and Operation of Aero Engines," Tech. Rep. CP-144, AGARD.

[10] Horlock, J., and Marsh, H., "Flow Models for Turbomachines," JOURNAL OF MECHANICAL ENGINEERING SCIENCES, Vol. 13, No. 5, 1971.

[11] Kerrebrock, J. L., Aircraft Engines and Gas Turbines, 2nd Ed., MIT Press, 1996.

[12] Jameson, A., Schmidt, W., Turkel, E., "Numerical Solutions of the Euler Equations by Finite Volume Methods Using Runge-Kutta Time-Stepping Schemes," AIAA Paper No. 81-1259, 1981.

[13] Lejambre, C. R., Zacharias, R. M., Biederman, B. P., Gleixner, A. J., and Yetka, C. J., "Development and Application of a Multistage Navier-Stokes Solver: Part II – Application to a High Pressure Compressor Design," ASME JOURNAL OF TURBOMACHNERY, Vol. 120, 1998, pp. 215-223.

[14] Longley, J. P., "Calculating the Flowfield Behaviour of High-Speed Multi-Stage Compressors," ASME Paper 97-GT-468, 1997.

[15] Marble, F. E., "Three-Dimensional Flow in Turbomachines," THE AERODYNAMICS OF AIRCRAFT ENGINES, edited by Sir W. Hawthorne, 1956.

[16] Mikolajczak, A., "The Practical Importance of Unsteady Flow," Tech. Rep. CP-144, AGARD.

[17] Mulac, R. A., and Adamczyk, J. J., "The Numerical Simulation of a High-Speed Axial Flow Compressor," ASME JOURNAL OF TURBOMACHNERY, Vol. 108, No. 2, 1986.

[18] Novak, R. A., "Streamline Curvature Computing Procedures for Fluid-Flow Problems," ASME JOURNAL OF ENGINEERING FOR POWER, Oct. 1967, pp. 478-490.

[19] Reid, C., "The Response of Axial Flow Compressors to Intake Flow Distortion," ASME Paper 69-GT-29, 1969.

[20] Reid, L., Moore, R. D., "Design and Overall Performance of Four Highly Loaded, High-Speed Inlet Stages for an Advanced High-Pressure-Ratio Core Compressor," NASA Technical Paper 1337, 1978.

[21] Rhie, C. M., Gleixner, A. J., Spear, D. A., Fischberg, C. J., and Zacharias, R M., "Development and Application of a Multistage Navier-Stokes Solver: Part I – Multistage Modeling Using Bodyforces and Deterministic stresses," ASME JOURNAL OF TURBOMACHNERY, Vol. 120 1998, pp. 205-214.

[22] Smith, L. H., "The Radial Equilibrium Equation of Turbomachinery," ASME JOURNAL OF ENGINEERING FOR POWER, Vol. 88, Jan. 1966, pp. 1-12.

[23] Smith, L. H., "Casing Boundary Layers in Axial Flow Compressors," FLOW RESEARCH OF BLADING, edited by L.S. Dzung, 1970.

[24] Sonin, A. A., "The Physical Basis of Dimensional Analysis", Class notes from MIT Course 2.25 – Advanced Fluid Mechanics, 1999.

[25] Valkov, T. "The Effect of Upstream Rotor Vortical Disturbances on the Time-Averaging Performance of Axial Compressor Stators," Ph.D. Dissertation, Massachusetts Institute of Technology, 1997.

[26] Wisna, A. I., "A Computational Model for Multistage Axial Compressor Design," M.S. Dissertation, Massachusetts Institute of Technology, 1998.